Vinyl Acetate Synthesis

Selective and Unselective Paths

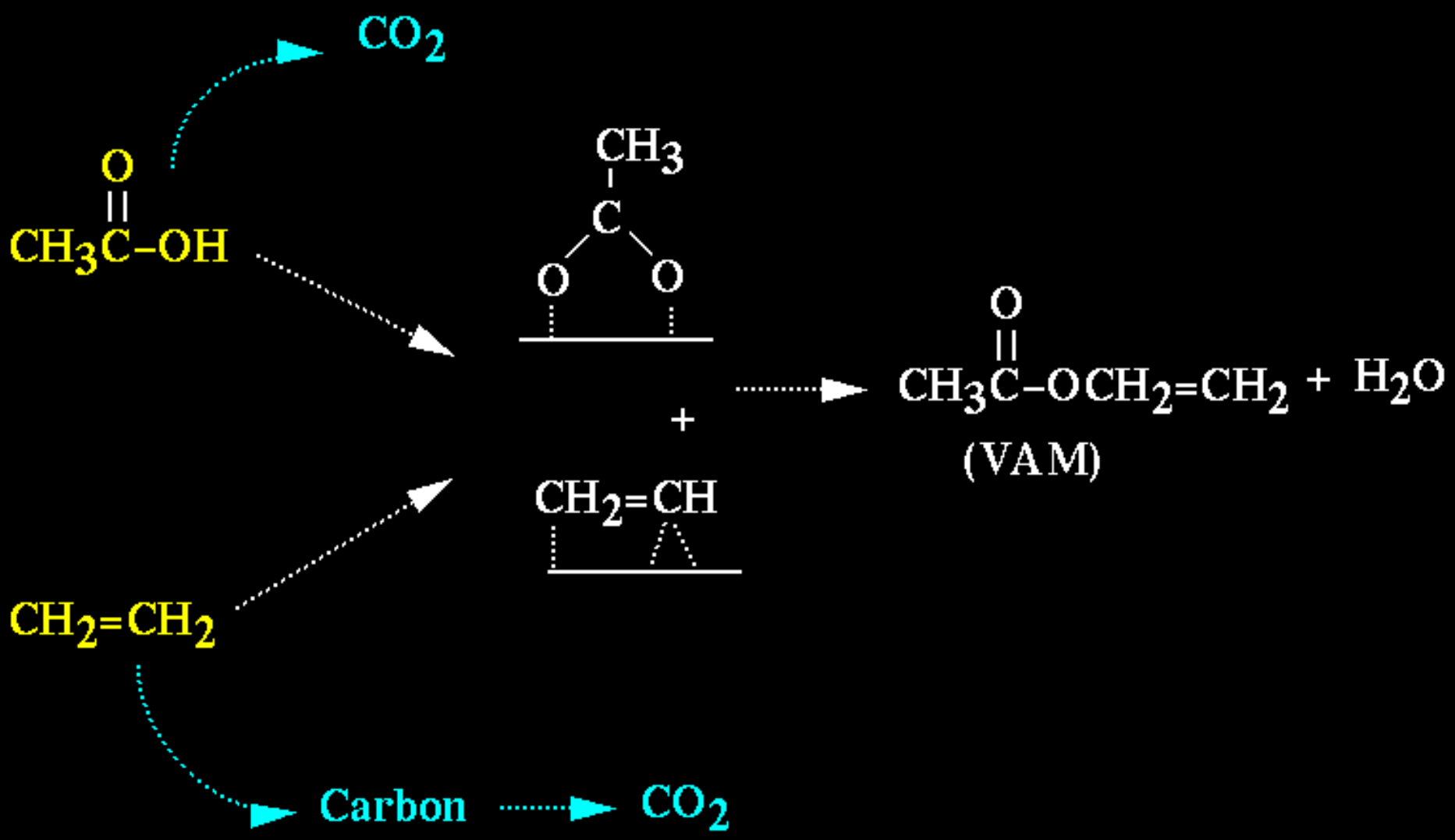

Neurock, M., J. Catal., 216 (1-2): 73-88, 2003.

Reaction Kinetics

Vinyl Acetate Synthesis

	ν_{for}	ν_{rev}	E_{for}	E_{rev}
$O_2 = O^* + O^*$	1	10^{13}	0.0	42.4
$H_2 = H^* + H^*$	0.1	10^{13}	6.9	19.7
$C_2H_4 = C_2H_4^*$	1	10^{9}	0.0	14.0
$MeCO_2H = MeCO_2H^*$	1	10^{13}	0.0	11.9
$MeCO_2H = MeCO_2^* + H^*$	1	10^{13}	0.0	14.3
$MeCO_2H + O^* = MeCO_2^* + OH^*$	1	10^{13}	0.0	20.1
$CO = CO^*$	1	10^{13}	0.0	35.1
$CO_2 = CO_2^*$	1	10^{13}	0.0	5.6
$H_2O = H_2O^*$	1	10^{13}	0.0	9.6
$MeCO_2CHCH_2 = MeCO_2^* + CHCH_2^*$	1	10^{13}	5.6	15.8
$MeCO_2CHCH_2 + H^* = MeCO_2^* + CHCH_2^*$	1	10^{13}	0.	25.3
$C_2H_4 = CHCH_2^* + H^*$	1	10^{13}	8.1	7.0
$C_2H_4 + O^* = CHCH_2^* + OH^*$	1	10^{13}	3.6	8.3
$OH^* = O^* + H^*$	10^{13}	10^{13}	20.8	15.0
$2\,OH^* = O^* + H_2O^*$	10^{13}	10^{13}	5.6	19.4
$CH^* = C^* + H^*$	10^{13}	10^{13}	32.5	11.2
$CH^* + O^* = C^* + OH^*$	10^{13}	10^{13}	34.0	18.4
$CH_2^* = CH^* + H^*$	10^{13}	10^{13}	17.3	26.2

	ν_{for}	ν_{rev}	E_{for}	E_{rev}
$CH_2^* + O^* = CH^* + OH^*$	10^{13}	10^{13}	11.1	25.8
$C_2H_4^* + O^* = CHCH_2^* + OH^*$	10^{13}	10^{13}	17.7	8.3
$C_2H_4^* = CHCH_2^* + H^*$	10^{13}	10^{13}	22.1	7.0
$CHCH_2^* = CH^* + CH_2^*$	10^{13}	10^{13}	27.9	24.3
$CHCH_2^* = H^* + CCH_2^*$	10^{13}	10^{13}	24.6	16.3
$CHCH_2^* + O^* = OH^* + CCH_2^*$	10^{13}	10^{13}	18.8	16.2
$MeCO_2H^* = MeCO_2^* + H^*$	10^{13}	10^{13}	12.8	15.2
$MeCO_2H^* + O^* = MeCO_2^* + OH^*$	10^{13}	10^{13}	1.1	9.3
$MeCO_2^* + O^* = CH_2CO_2^* + OH^*$	10^{13}	10^{13}	18.7	12.1
$MeCO_2^* = CH_2CO_2^* + H^*$	10^{13}	10^{13}	23.9	11.5
$CH_2CO_2^* = CH_2 + CO_2^*$	10^{13}	10^{13}	6.3	0.0
$CHCH_3^* = CHCH_2^* + H^*$	10^{13}	10^{13}	15.7	13.3
$CHCH_3^* + O^* = CHCH_2^* + OH^*$	10^{13}	10^{13}	17.5	20.9
$CHCH_3^* = CCH_3^* + H^*$	10^{13}	10^{13}	14.8	29.6
$CHCH_3^* + O^* = CCH_3^* + OH^*$	10^{13}	10^{13}	8.5	29.1
$CCH_3^* = CCH_2^* + H^*$	10^{13}	10^{13}	33.2	7.7
$CCH_3^* + O^* = CCH_2^* + OH^*$	10^{13}	10^{13}	36.7	16.9
$CO^* = C^* + O^*$	10^{13}	10^{13}	70.6	0.0
$CCH_2^* = CH_2^* + C^*$	10^{13}	10^{13}	34.5	18.0
$CO_2^* = CO^* + O^*$	10^{13}	10^{13}	32.6	0.0

Neurock, M., J. Catal., 216 (1-2): 73-88, 2003.

DFT–Predicted Reaction Energetics

Ethylene Hydrogenation on Palladium

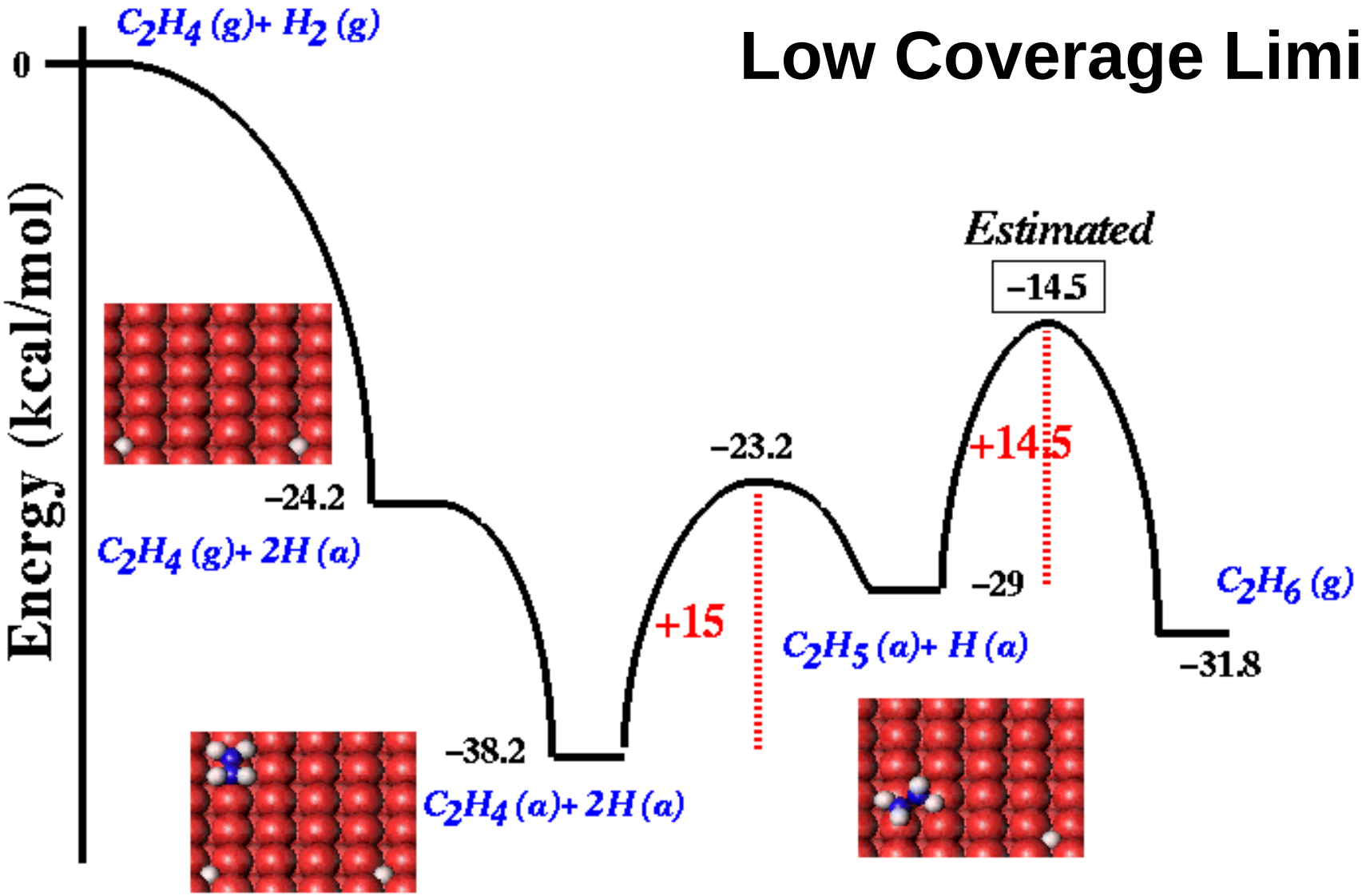

Surface Coverage Effects

Stabilizing Transient Reaction Intermediates

Transient π-Bound Ethylene Intermediate
Responsible for facile hydrogenation

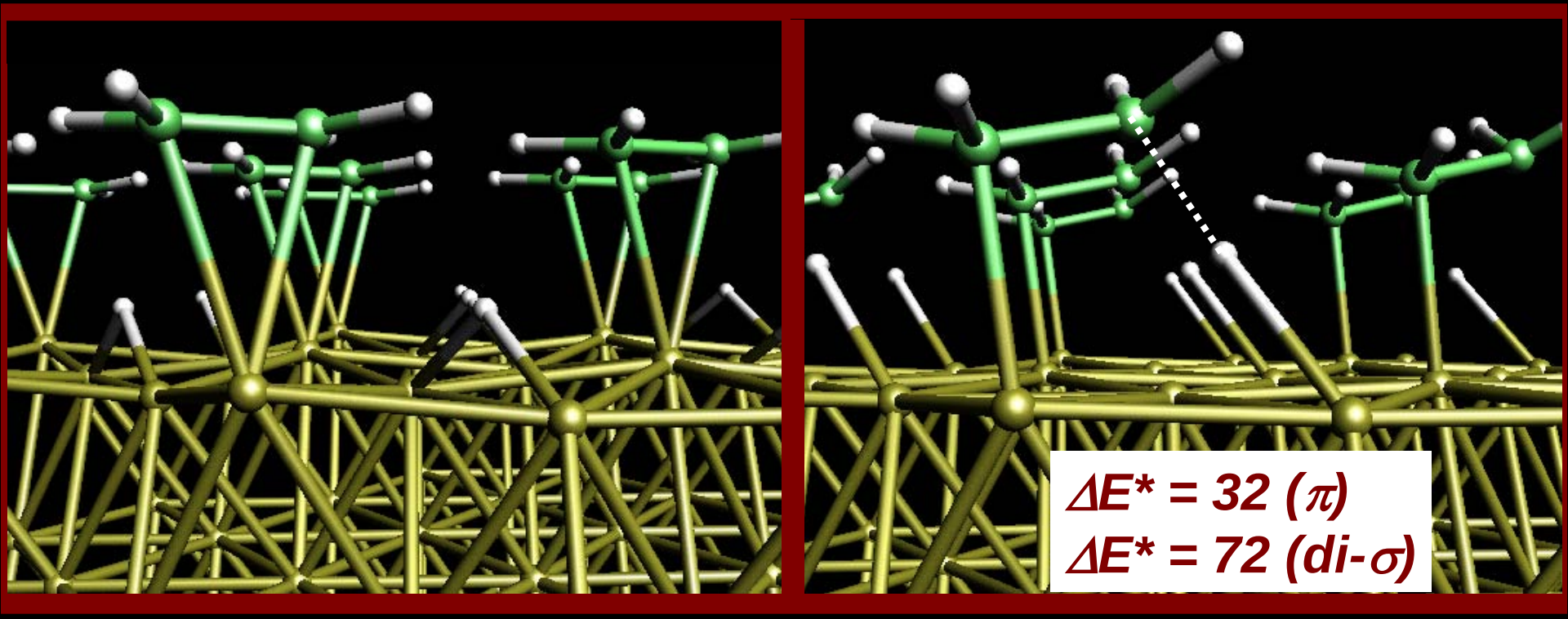

di-σ intermediate can lead to ethylidyne

Neurock, M., P.S. Venkataraman, and R.A. van Santen, J. Am. Chem. Soc., 122(6):1150-1153, 2000.

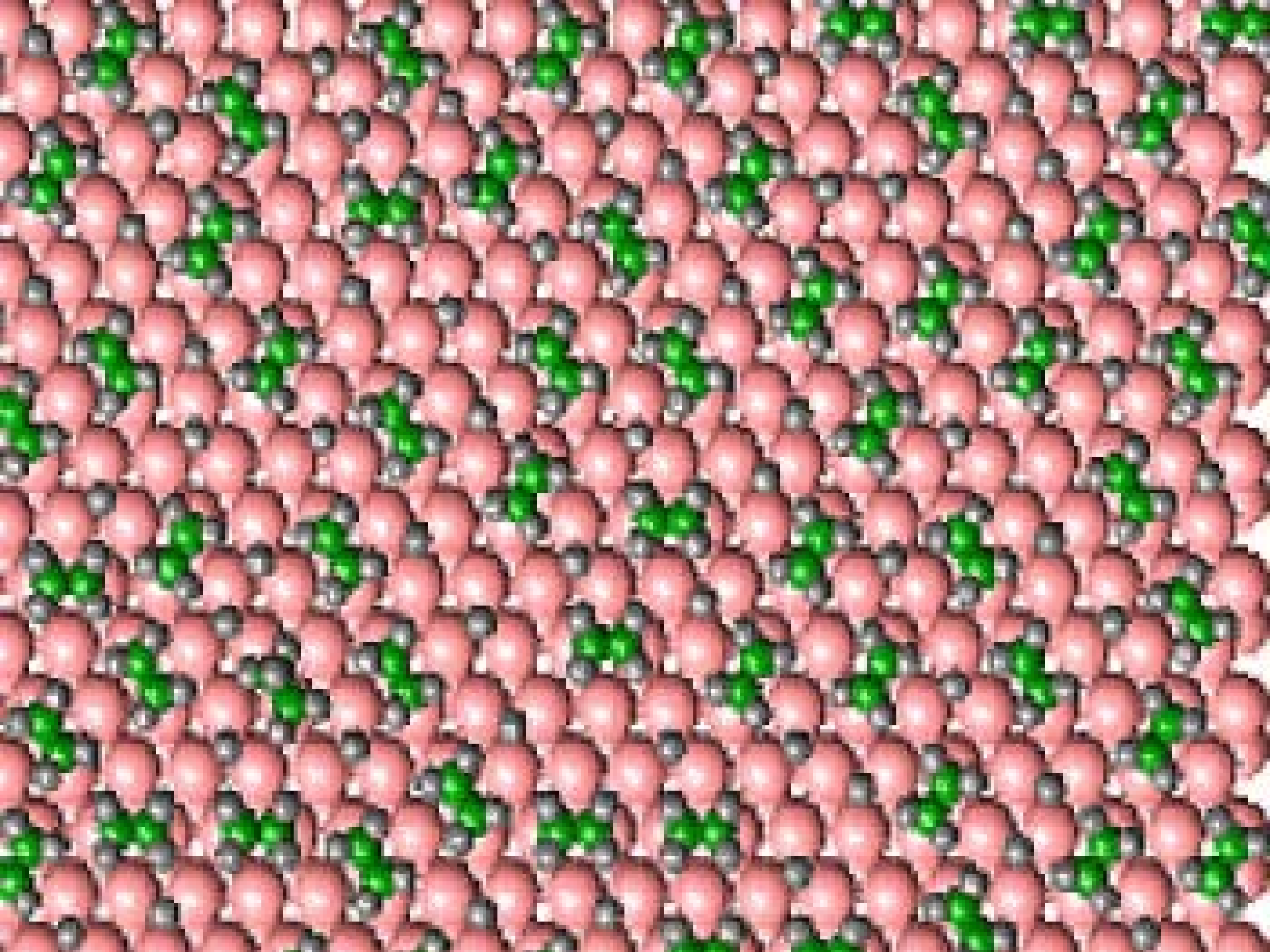

Ethylene Hydrogenation Results

Simulations on Pd(111):

$$R_{Ethane} = 10^{5.4\pm0.7} \cdot \exp\left(\frac{-9.5\pm2.5\,kcal/mol}{R\cdot T}\right) \cdot P_{H_2}^{0.65-1} \cdot P_{C_2H_4}^{-0.4-0}$$

Experiments on Supported Pd :

$$R_{Ethane} = 10^{6.3} \cdot \exp\left(\frac{-8.5\pm2.5\,kcal/mol}{R\cdot T}\right) \cdot P_{H_2}^{0.5-1} \cdot P_{C_2H_4}^{-0.3-0}$$

Factors Influencing Turnover Frequencies

Ethylene Hydrogenation on Palladium

	Turn–over Frequency	H* Coverage (ML)	$E_{ads}(H^*)$ (kcal/mol)	$E_{ads}(C_2H_4^*)$ (kcal/mol)	$C_2H_4^*$ Coverage (ML)
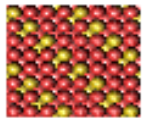	0.10	0.15	60.0	10.7	0.1875
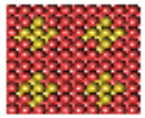	0.10	0.27	61.6	9.7	0.176
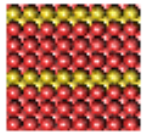	0.13	0.25	62.3	9.3	0.184
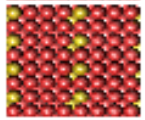	0.11	0.29	61.3	8.5	0.179
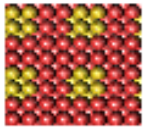	0.13	0.27	61.3	10.3	0.176
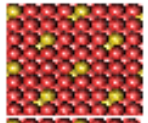	0.15	0.28	61.2	9.1	0.18
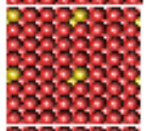	0.14	0.36	62.1	9.1	0.19
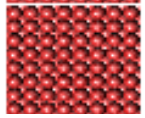	0.14	0.42	62.5	9.1	0.182

Decreasing

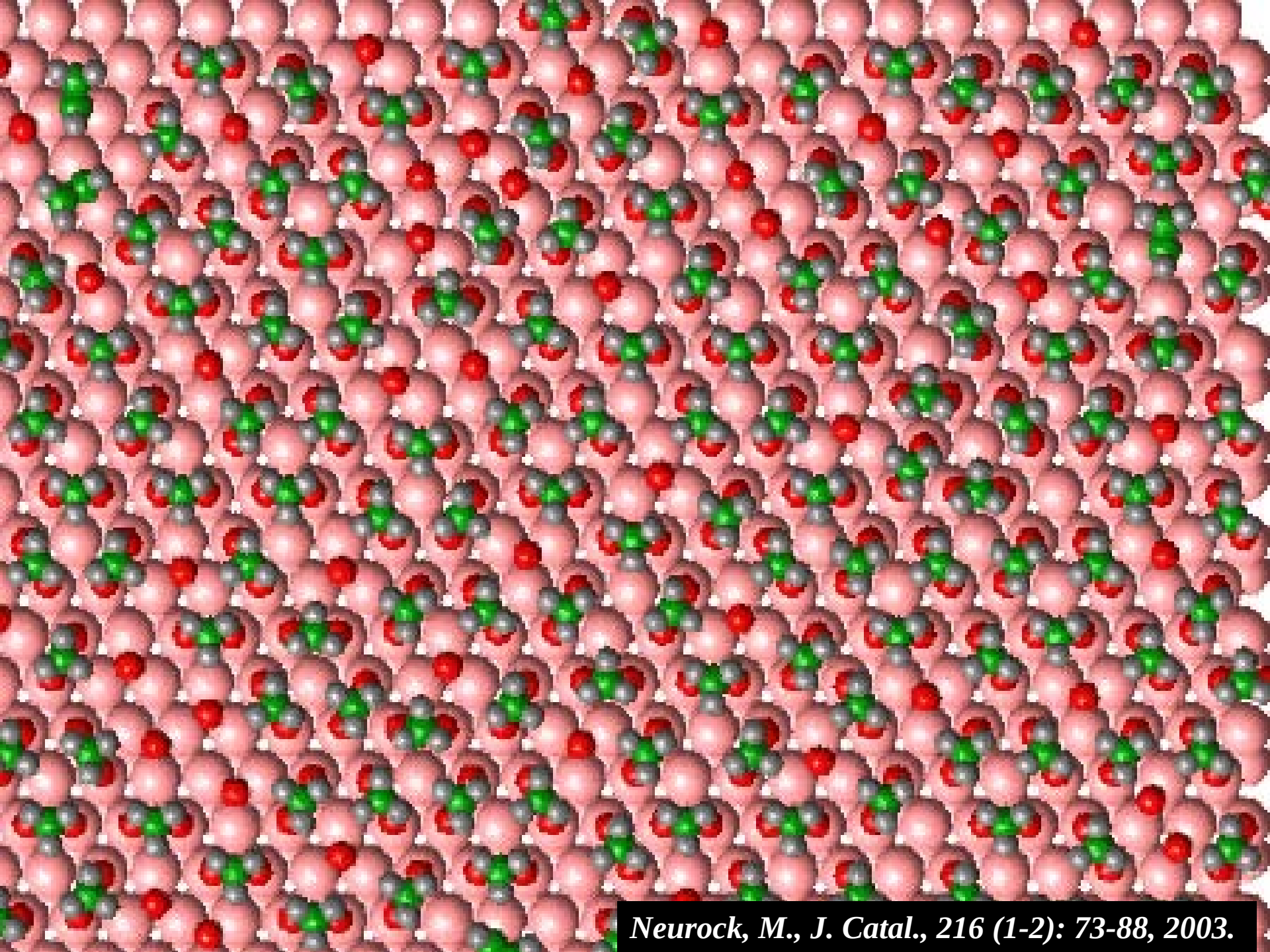

Neurock, M., J. Catal., 216 (1-2): 73-88, 2003.

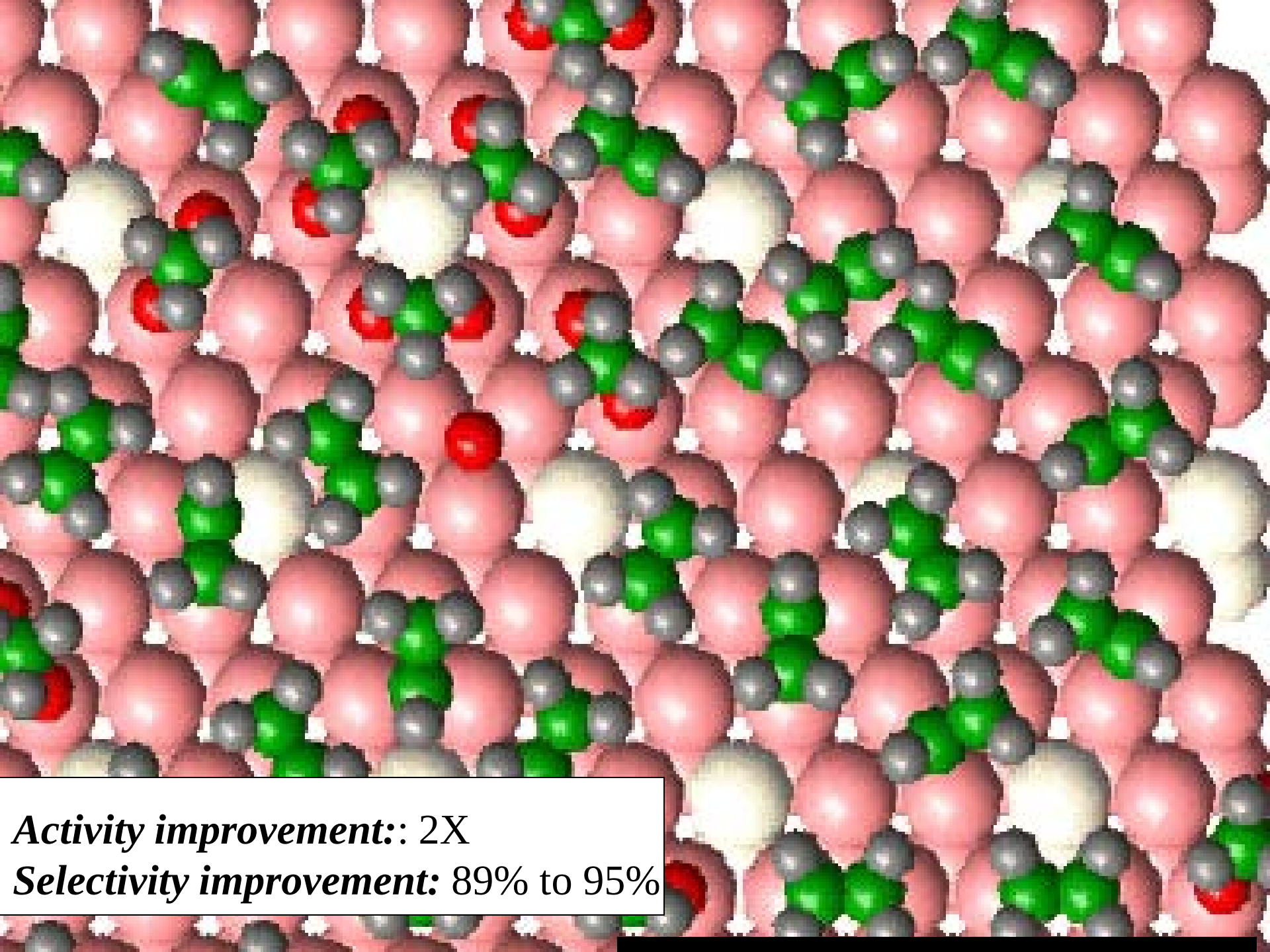

Activity improvement:: 2X
Selectivity improvement: 89% to 95%

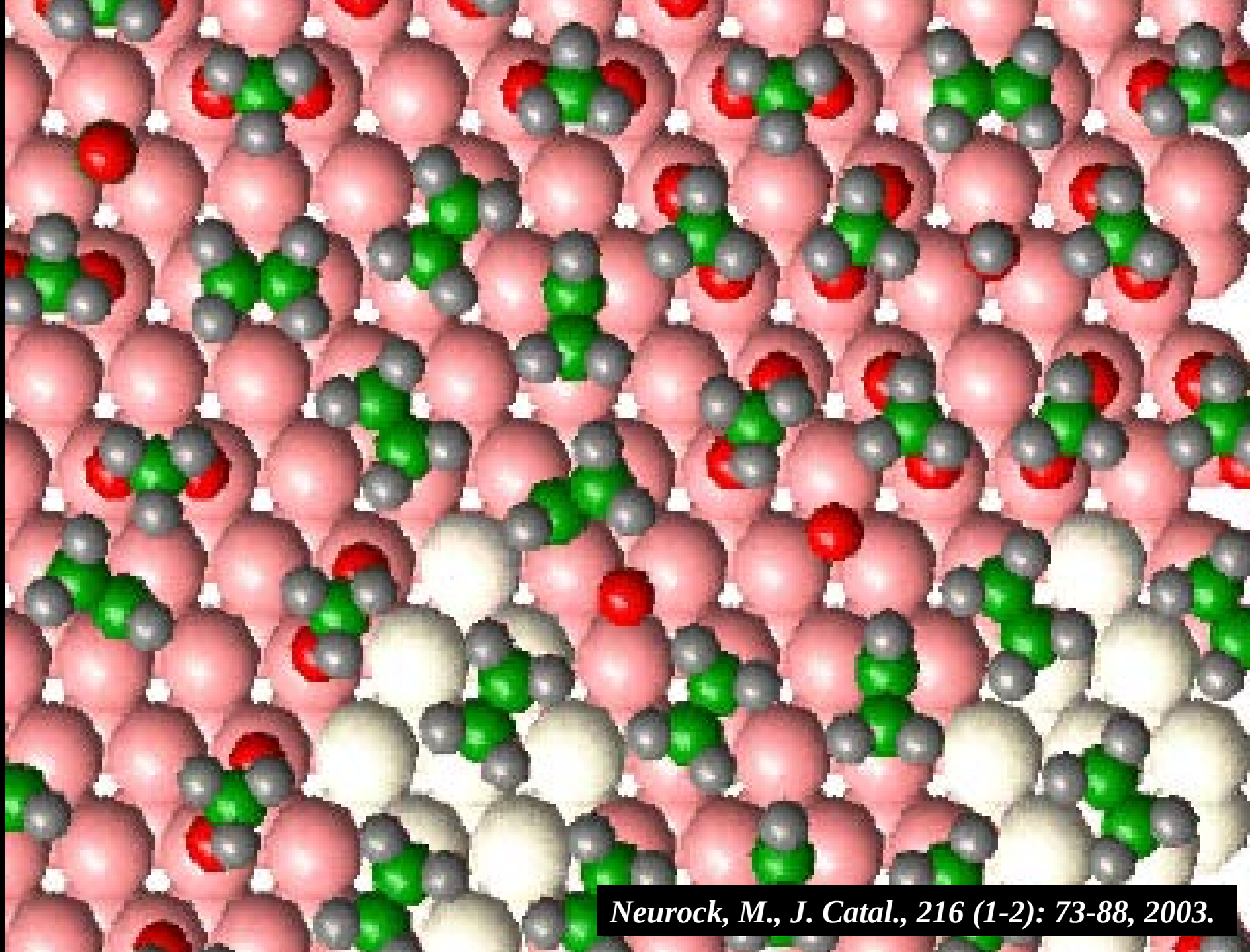

Neurock, M., J. Catal., 216 (1-2): 73-88, 2003.

Acetylene Hydrogenation

Ethylene feeds contain as high as 1% acetylene.

Acetylene leads to deleterious processing issues.

Processing requires < few ppm of acetylene.

Over-hydrogenation leads to:

- ***Temperature excursions***
- ***Poor selectivity***
- ***Deactivation***

Control of the selectivity to ethylene is critical.

Acetylene Hydrogenation Reaction Paths

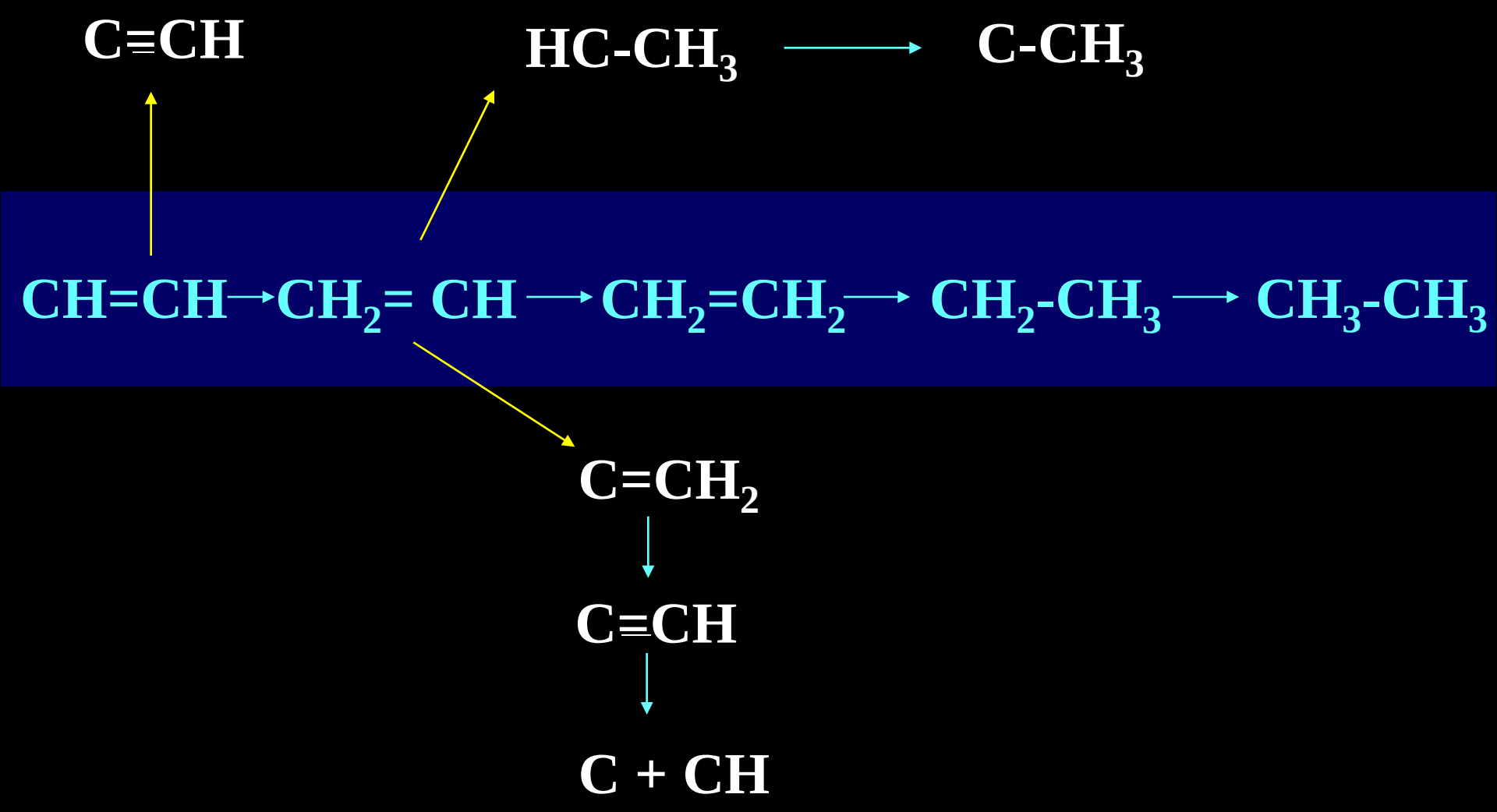

Energy Diagram for Acetylene Hydrogenation over Pd(111)

Sheth, P., S. Desai, and M. Neurock, J. Phys. Chem., 107 (9): 2009-2017, (2003).

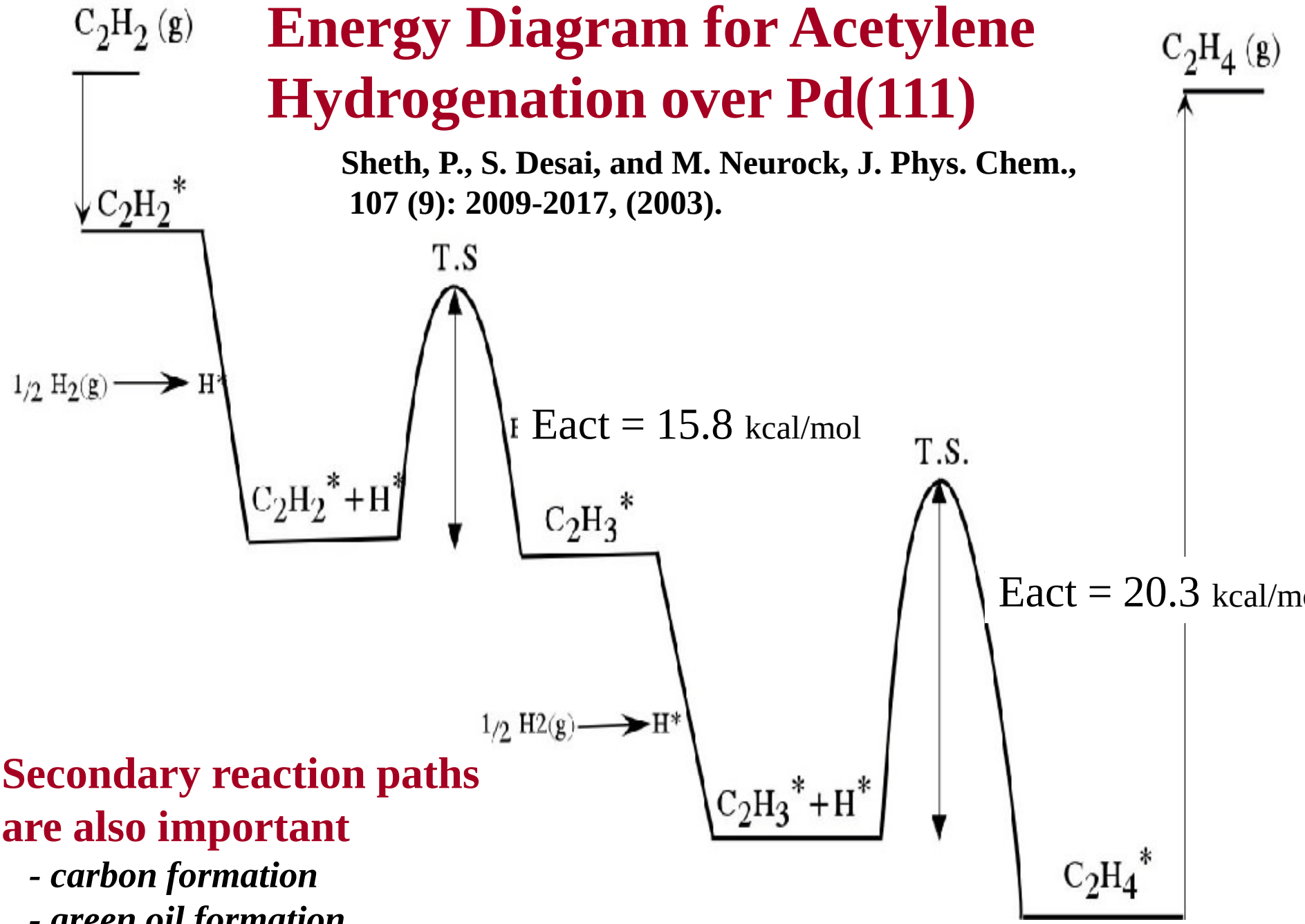

Secondary reaction paths are also important

- ***carbon formation***
- ***green oil formation***

DFT–Predicted Reaction Energetics

Ethylene Hydrogenation on Palladium

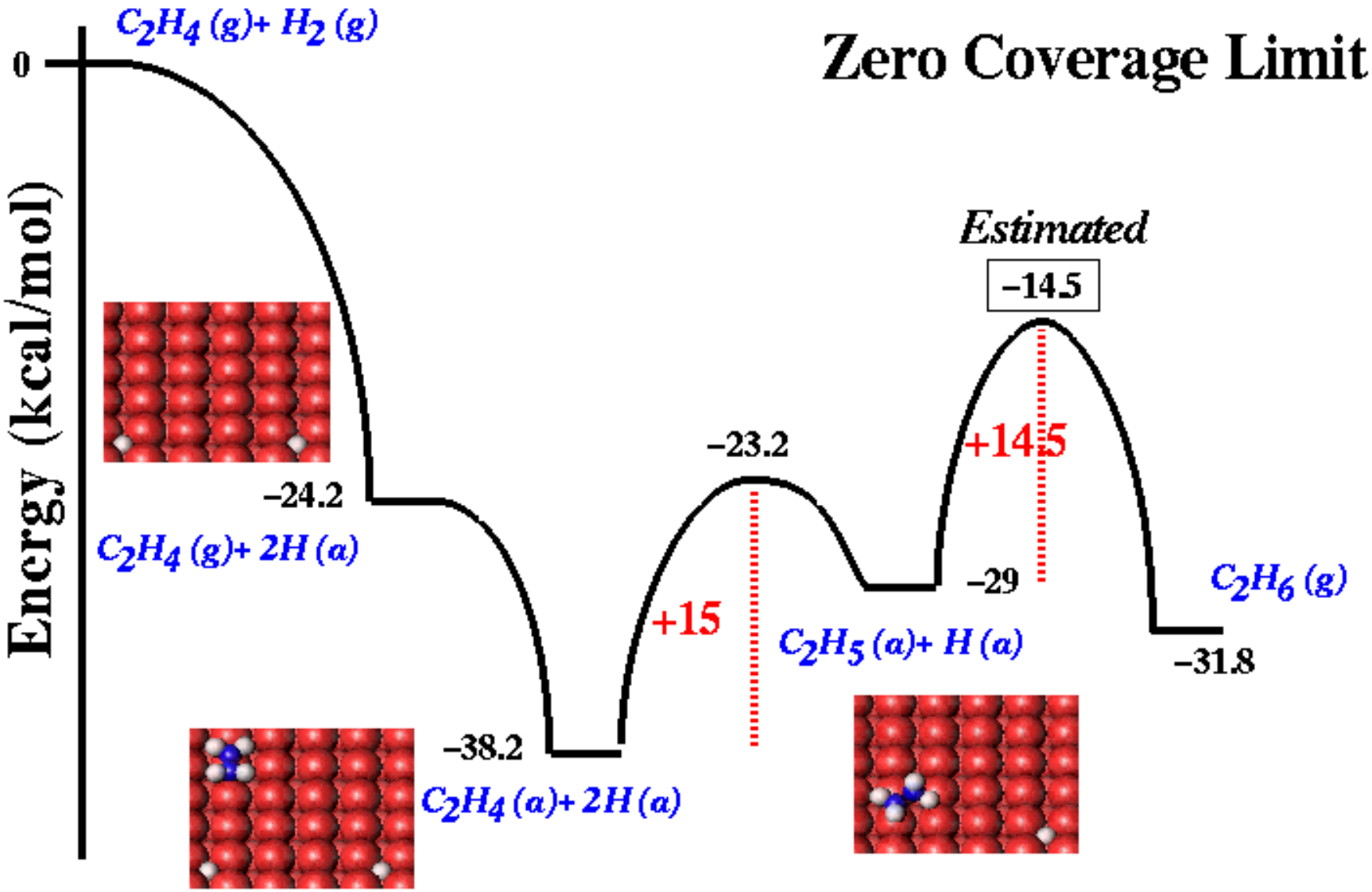

Acetylene Hydrogenation

Conditions

T= 300-500 K

P_{C2H2} = 5-100 torr
P_{H2} = 100-600 torr

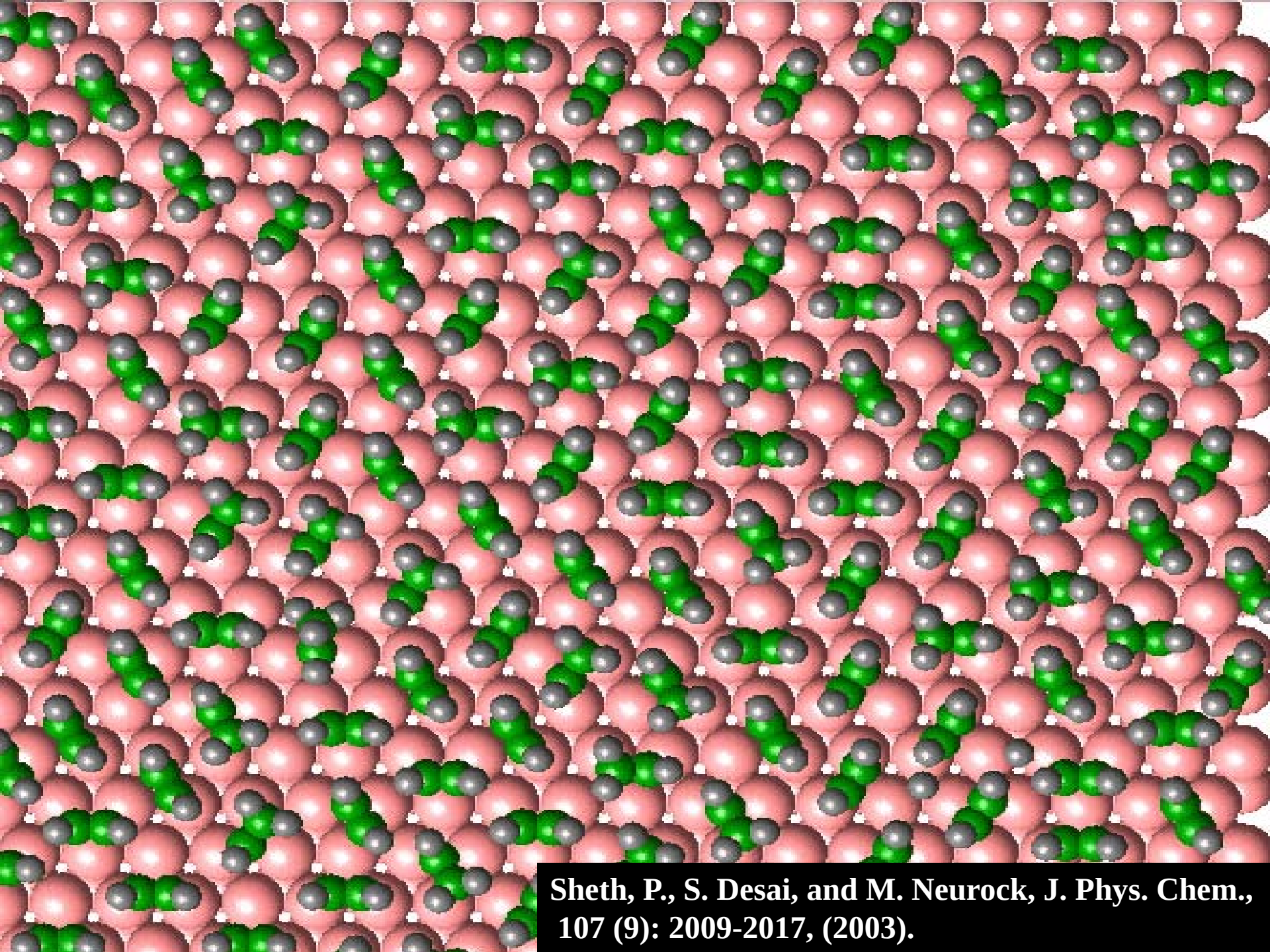

Sheth, P., S. Desai, and M. Neurock, J. Phys. Chem., 107 (9): 2009-2017, (2003).

Arrhenius Plot - Acetylene Hydrogenation

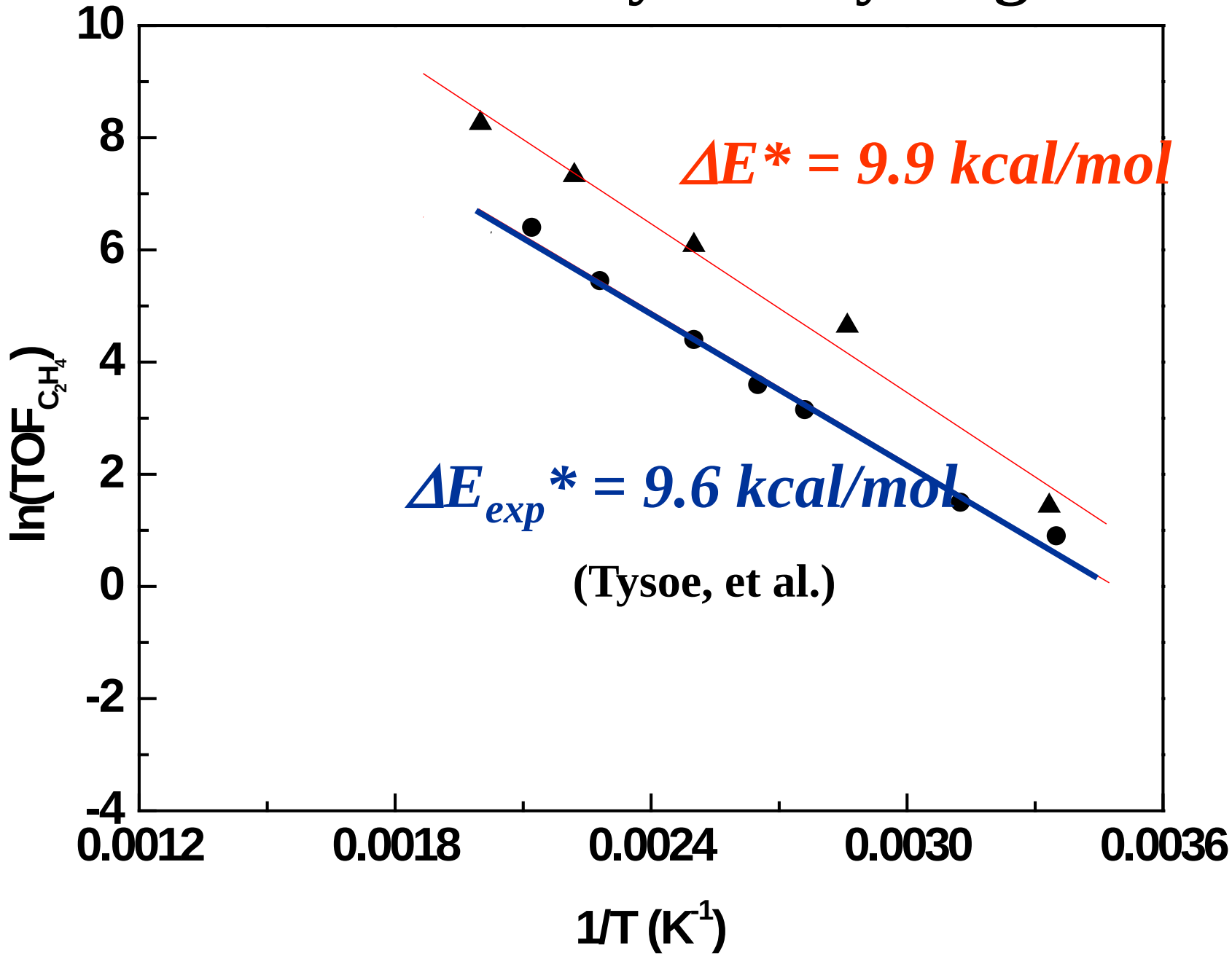

Simulated Reaction Orders

$r \alpha P_{C2H2}^{-0.52} P_{H2}^{1.10}$ *DFT*

$r \alpha P_{C2H2}^{-0.65} P_{H2}^{1.05}$ *Experiment*

Selectivity to Ethylene

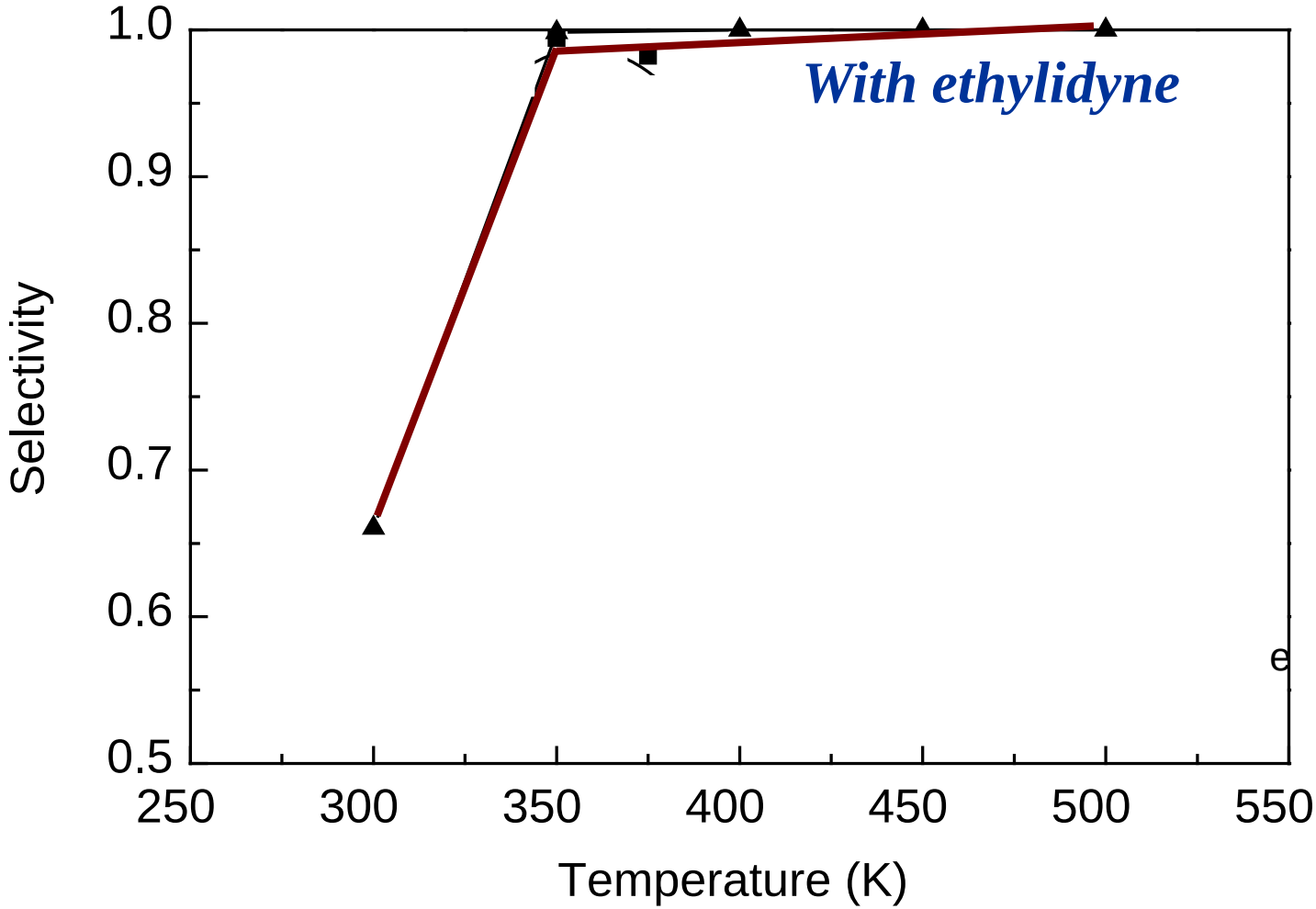

Compares with experiments (30% at 300 K and 90% at 500K)

However, no paths are included for benzene formation.

Effect of Alloying

Sheth, P. A., M. Neurock, and C.M. Smith,
J. Phys. Chem. B., 109 (25): 12449-12466. 2005

Promotes Hydrogenation

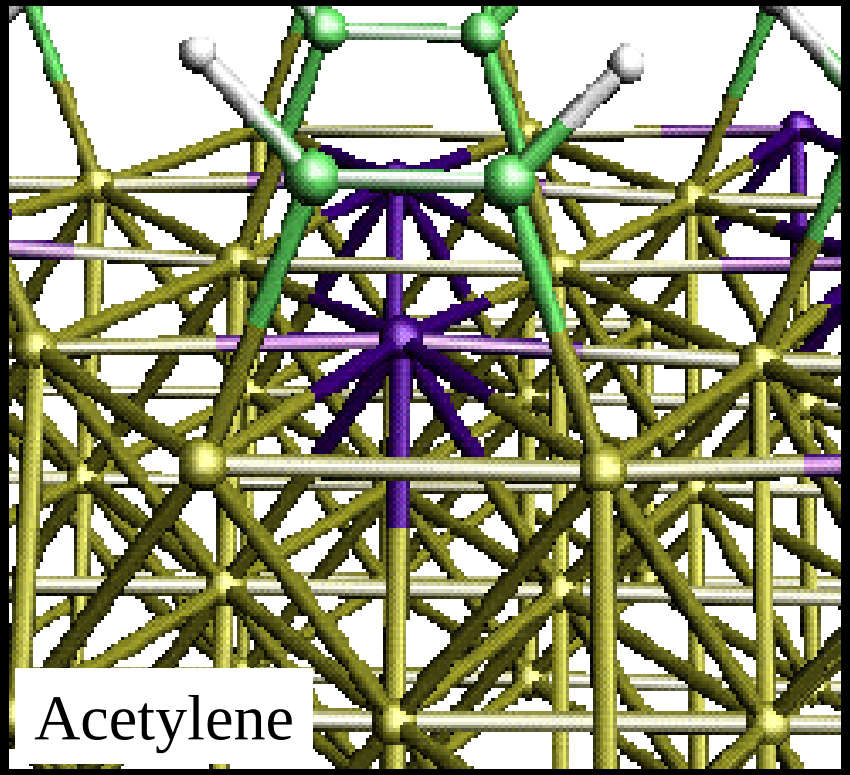

$\Delta(\Delta Eads) = +70$ kJ/mol

$\Delta E_{ads} = 55$ kJ/mol

Promotes Desorption

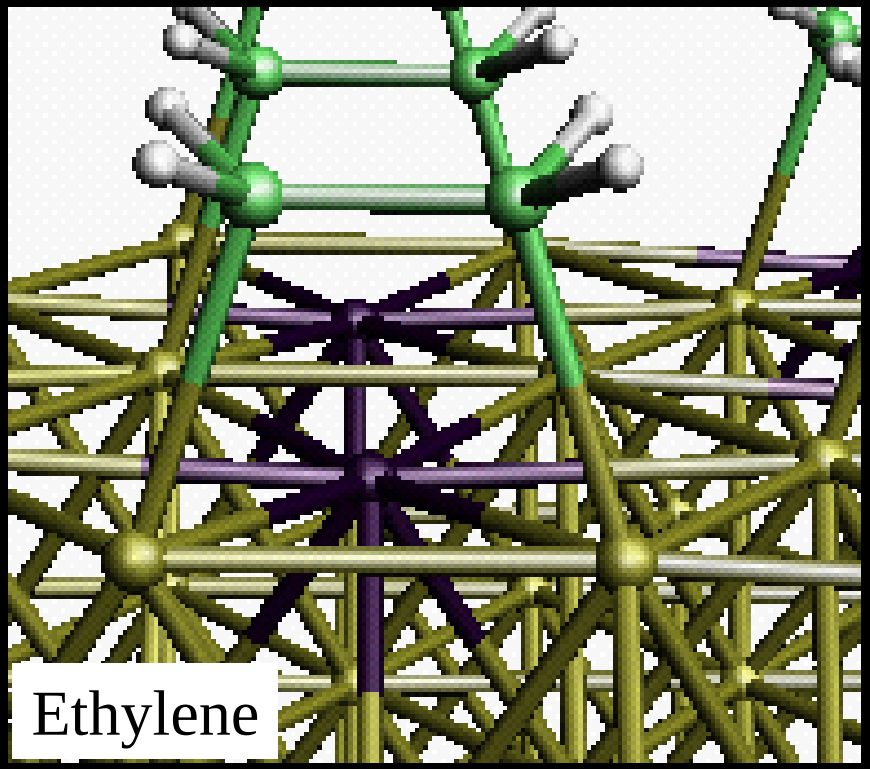

$\Delta(\Delta Eads) = +30$ kJ/mol

$\Delta E_{ads} = 20$ kJ/mol

Alloying Effects

Geometric and electronic effects

Hydrogenation becomes more exothermic with increasing Ag.

Bond activation steps more endothermic with increasing Ag.

Hydrogenation > C-H activation > C-C bond activation

Energetics strongly depend on the actual sites.

Ag increases the desorption of ethylene.

Manipulating the Reaction Environment

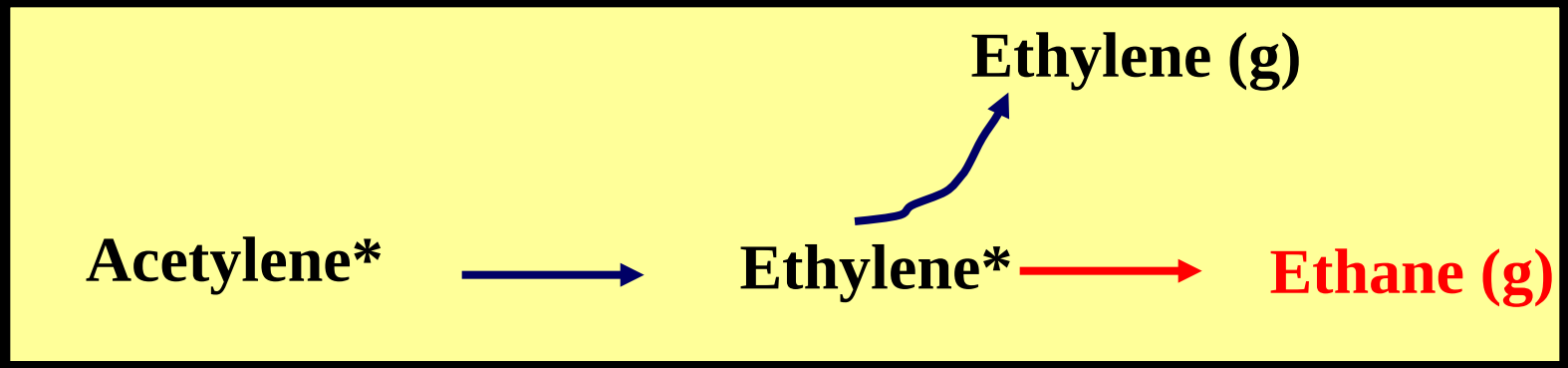

Balance of Geometric and Electronic Effects

Selectively inhibit3-fold sites.
Maintain bridge sites.
Increase hydrogen.
Decrease acetylene.
Weaken CxHy and H* binding energies.*

Methods

PdAg, PdAu or PdCu Alloys
Increased Coverage
Addition of CO

Deterministic Model Equations

Elementary Reactions

Adsorption Steps

$C_2H_2(g) + * \longleftrightarrow C_2H_2*$

$H_2(g) + 2* \longleftrightarrow 2H*$

$C_2H_4* \longleftrightarrow C_2H_4(g) + *$

Hydrogenation Steps

$C_2H_2* + H* \longleftrightarrow C_2H_3* + *$

$C_2H_3* + H* \longleftrightarrow C_2H_4* + *$

$C_2H_4* + H* \longleftrightarrow C_2H_5* + *$

$C_2H_5* + H* \longleftrightarrow C_2H_6 + 2*$

Decomposition Steps

$C_2H_3* + H* \longleftrightarrow HCCH_3* + *$

$C_2H_3* + * \longleftrightarrow CCH_2* + H*$

$CCH_2* + H* \longleftrightarrow CCH_3* + *$

Differential Equations

$$\frac{d}{dt}C_{C_2H_2} = \mathbf{k}_2 P_{C_2H_2} C_{vac} - \mathbf{k}_{-2} C_{C_2H_2} - \mathbf{k}_6 C_{C_2H_2} C_H + \mathbf{k}_{-6} C_{C_2H_3} C_{vac}$$

$$\frac{d}{dt}C_{C_2H_4} = \mathbf{k}_3 P_{C_2H_4} C_{vac} - \mathbf{k}_{-3} C_{C_2H_4} - \mathbf{k}_7 C_{C_2H_3} C_H + \mathbf{k}_{-7} C_{C_2H_4} C_{vac} - \mathbf{k}_8 C_{C_2H_4} C_H + \mathbf{k}_{-8} C_{C_2H_5} C_{vac}$$

$$\frac{d}{dt}C_{C_2H_6} = \mathbf{k}_4 P_{C_2H_6} C_{vac} - \mathbf{k}_{-4} C_{C_2H_6} - \mathbf{k}_9 C_{C_2H_5} C_H + \mathbf{k}_{-9} C_{C_2H_6} C_{vac}$$

$$\frac{d}{dt}C_{C_2H_3} = \mathbf{k}_6 C_{C_2H_2} C_H - \mathbf{k}_{-6} C_{C_2H_3} C_{vac} - \mathbf{k}_7 C_{C_2H_3} C_H + \mathbf{k}_{-7} C_{C_2H_4} C_{vac} - \mathbf{k}_{10} C_{C_2H_3} C_{vac} + \mathbf{k}_{-10} C_{CHCH_5} C_{vac}$$

$$\frac{d}{dt}C_{C_2H_5} = \mathbf{k}_8 C_{C_2H_4} C_H - \mathbf{k}_{-8} C_{C_2H_5} C_{vac} - \mathbf{k}_9 C_{C_2H_5} C_H + \mathbf{k}_{-9} C_{C_2H_6} C_{vac}$$

$$\frac{d}{dt}C_{CHCH_3} = \mathbf{k}_{10} C_{C_2H_3} C_H - \mathbf{k}_{-10} C_{CHCH_3} C_{vac} - \mathbf{k}_{11} C_{CHCH_3} C_{vac} + \mathbf{k}_{-11} C_{CCH_3} C_H$$

$$\frac{d}{dt}C_{CCH_3} = \mathbf{k}_{11} C_{CHCH_3} C_{vac} - \mathbf{k}_{-11} C_{CCH_3} C_H + \mathbf{k}_{13} C_{CCH_2} C_H + \mathbf{k}_{-13} C_{CCH_3} C_{vac}$$

$$\frac{d}{dt}C_{CCH_2} = \mathbf{k}_{12} C_{C_2H_3} C_{vac} - \mathbf{k}_{-12} C_{CCH_2} C_H - \mathbf{k}_{13} C_{CCH_2} C_H + \mathbf{k}_{-13} C_{CCH_3} C_{vac}$$

$$\frac{d}{dt}P_{C_2H_4} = \mathbf{k}_{-3} C_{C_2H_4} - \mathbf{k}_3 P_{C_2H_4} C_{vac}$$

$$\frac{d}{dt}P_{C_2H_6} = \mathbf{k}_{-4} C_{C_2H_6} - \mathbf{k}_4 P_{C_2H_6} C_{vac}$$

$$\frac{d}{dt}P_{H_2} = \mathbf{k}_{-1} C_H^{\ 2} - \mathbf{k}_1 P_{H_2} C_{vac}$$

Inclusion of Lateral Interaction Effects into Kinetic Model

First Principle Based Monte-Carlo Simulation

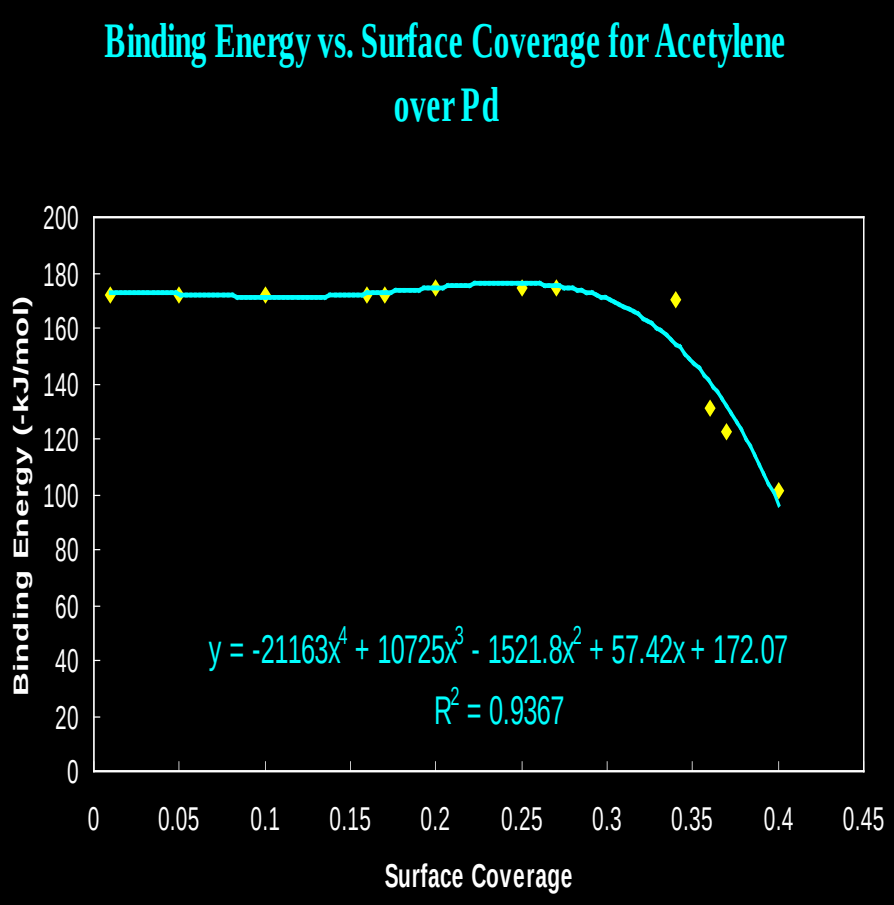

$$K=\exp(-\Delta G/RT)$$

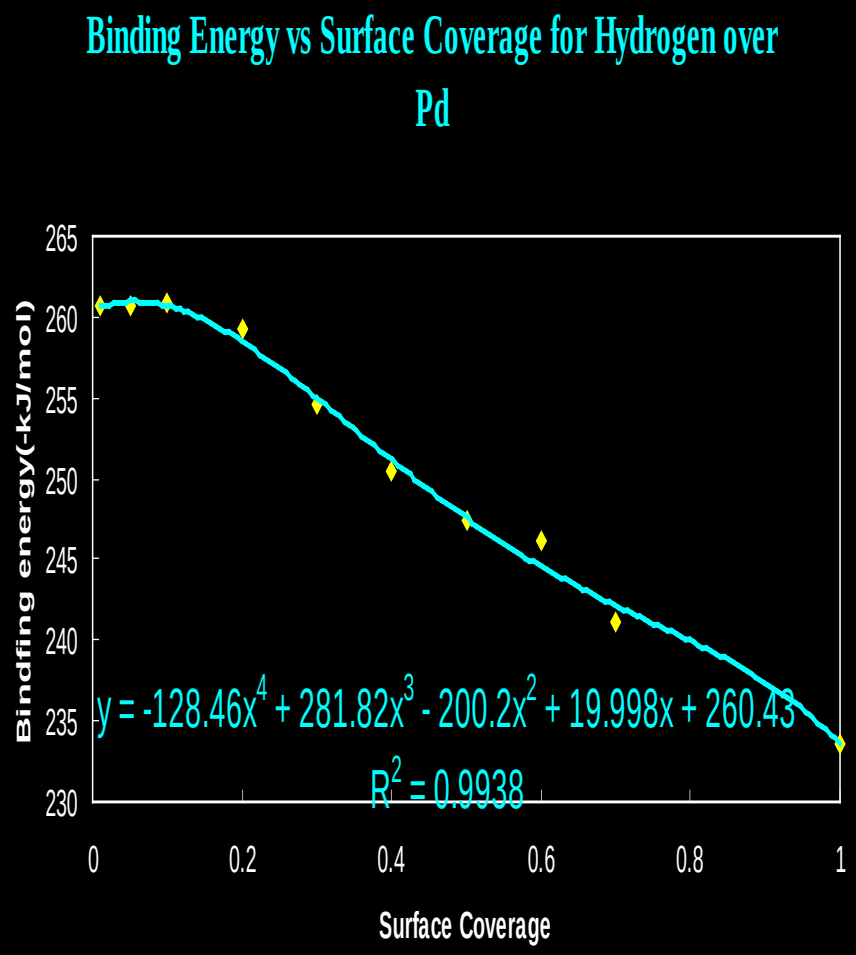

Dual-Site Model Results

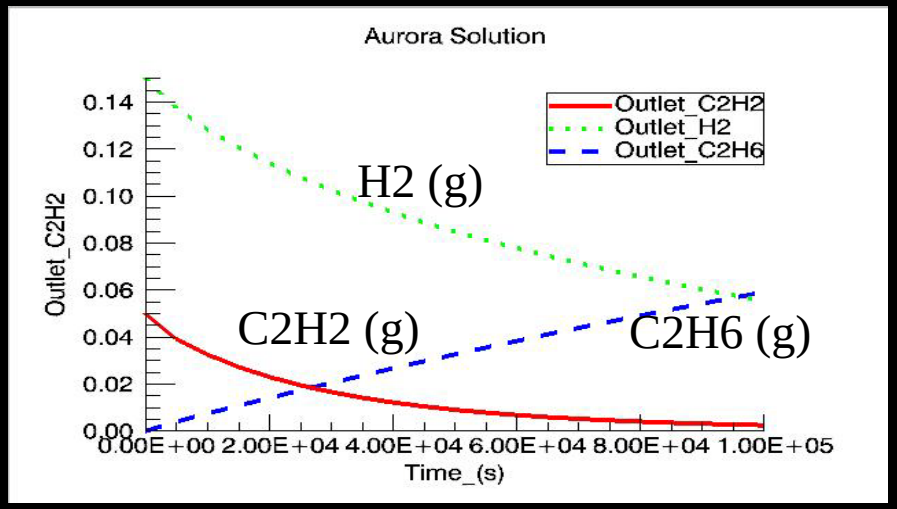

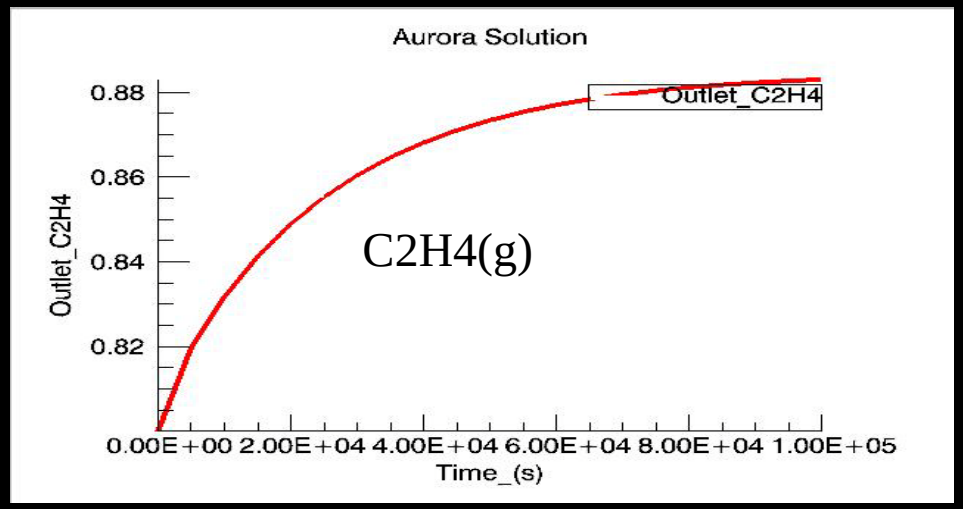

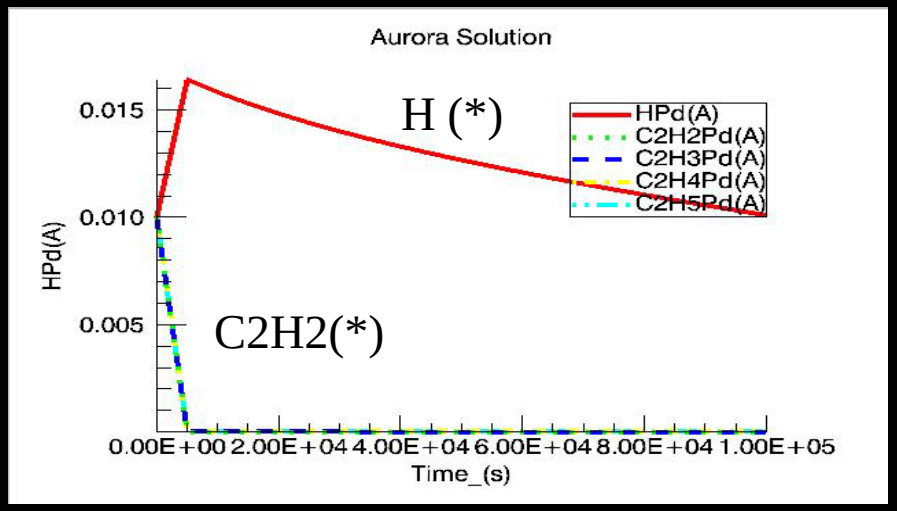

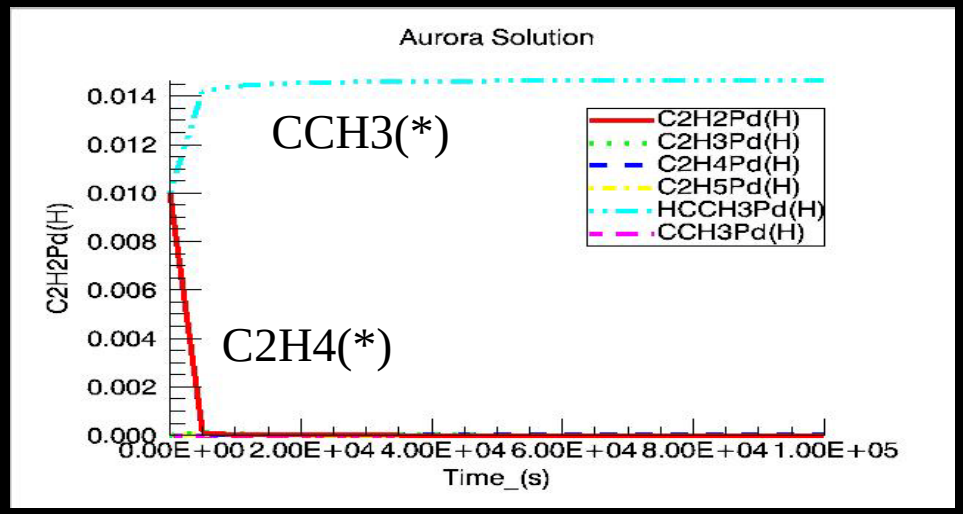

Activity maintained in spite of carbonaceous deposit formation

Second site maintains turn-over

CO Oxidation

General Model

Basic – Ziff – Gulari – Barshad (ZGB) Model

A = CO
B = O_2

$$A(g) + * \longrightarrow A^*$$

$$B_2(g) + 2^* \longrightarrow 2B^*$$

$$A^* + B^* \longrightarrow AB(g) + 2^*$$

Captures Interesting Phase Behavior

Continuous and Discontinuous Kinetic Phase Transitions

R.M. Ziff, E. Gulari, and Y. Barshad, Phys. Rev. Lett., 56, 1986, 2553.

Steady State Coverage of CO and O as a Function of $Y = P_A/(P_A+P_B)$

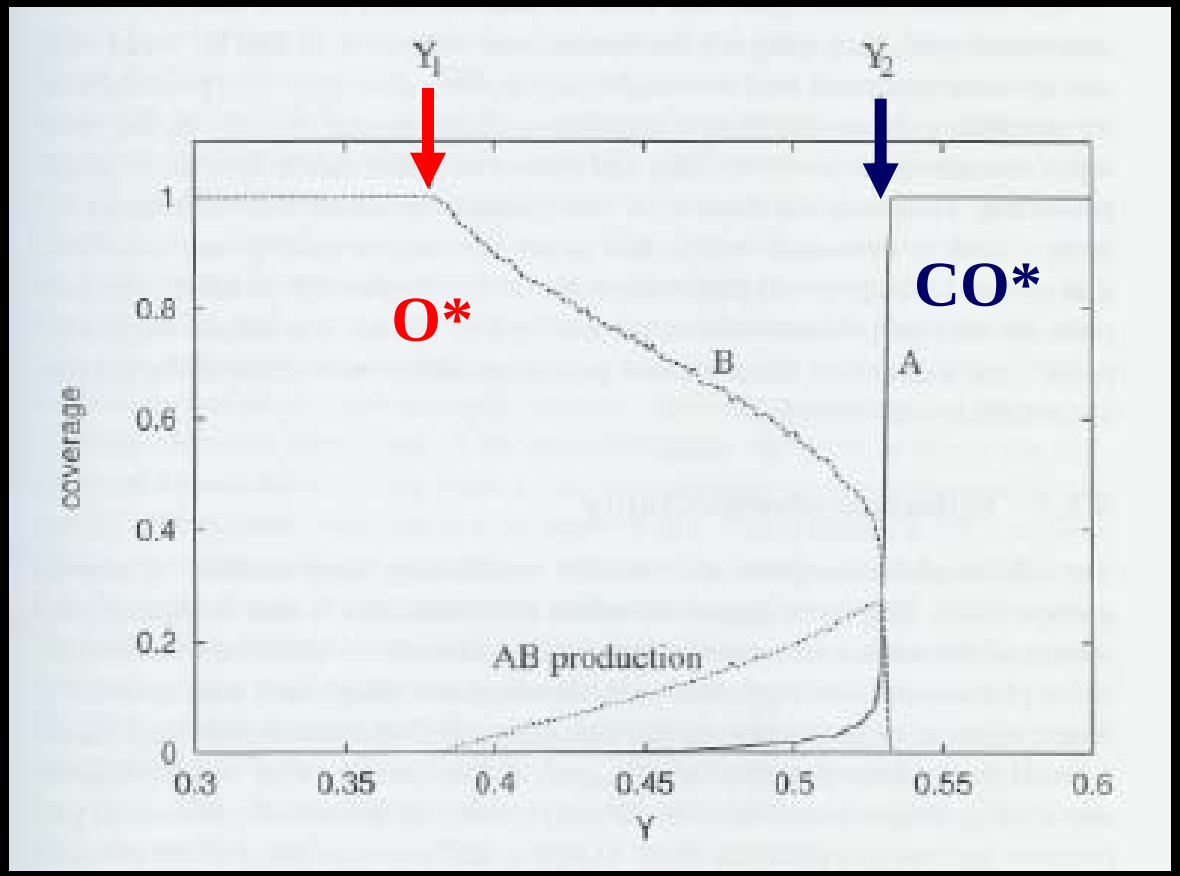

Later Expanded to Include Effects of:

- ***Desorption***
- ***Lateral Interactions***
- ***Diffusion.***
- ***Mechanism.***
- ***Surface Reconstruction***

R.M. Ziff, E. Gulari, and Y. Barshad, Phys. Rev. Lett., 56, 1986, 2553.

Kinetic Oscillation Observed

Result from the changes in surface coverages.

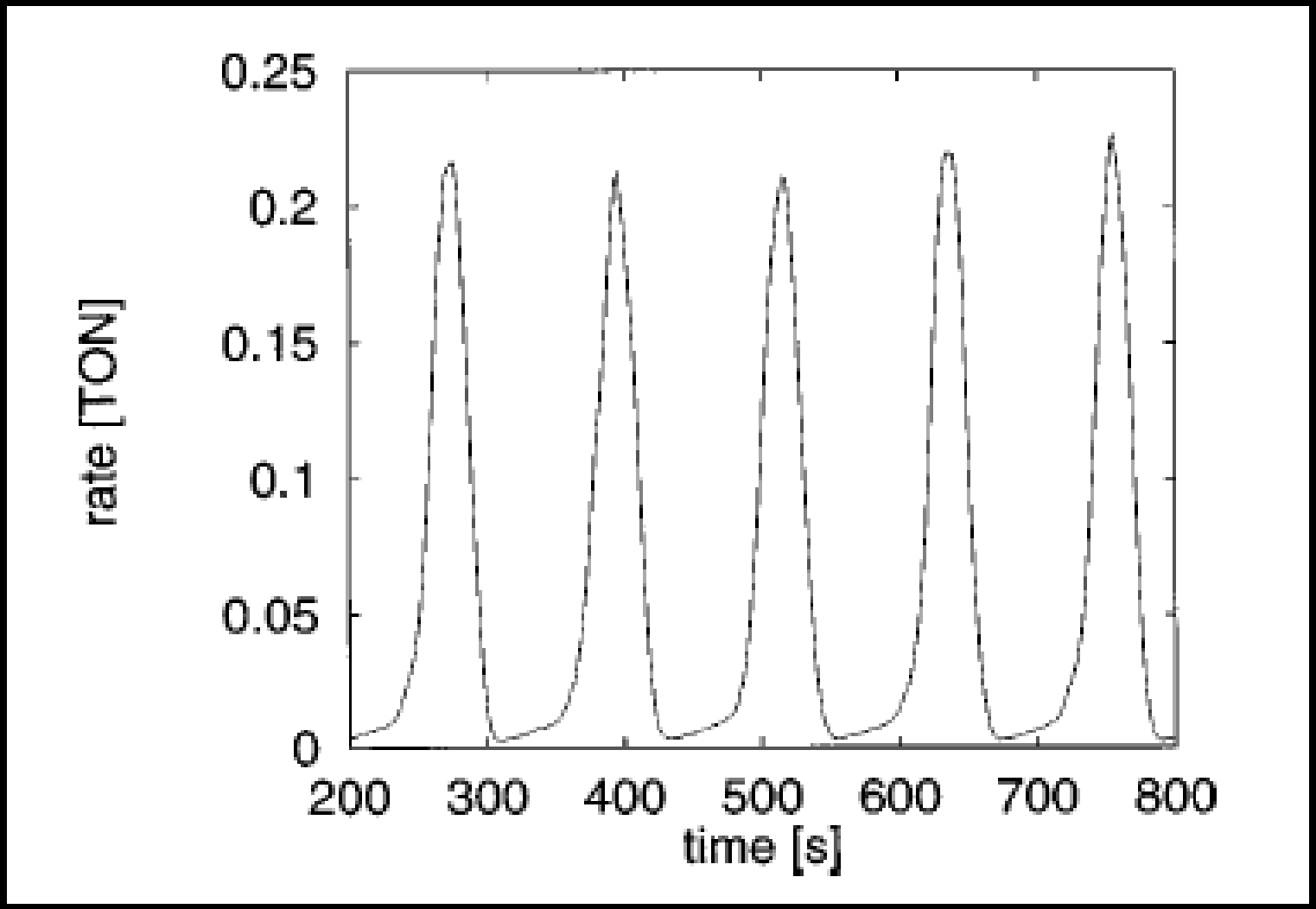

Gelten RJ, Jansen APJ, van Santen RA, et al., J. Chem. Phys. 108 (14) 5921-5934 1998

Kinetic Oscillations and Waves

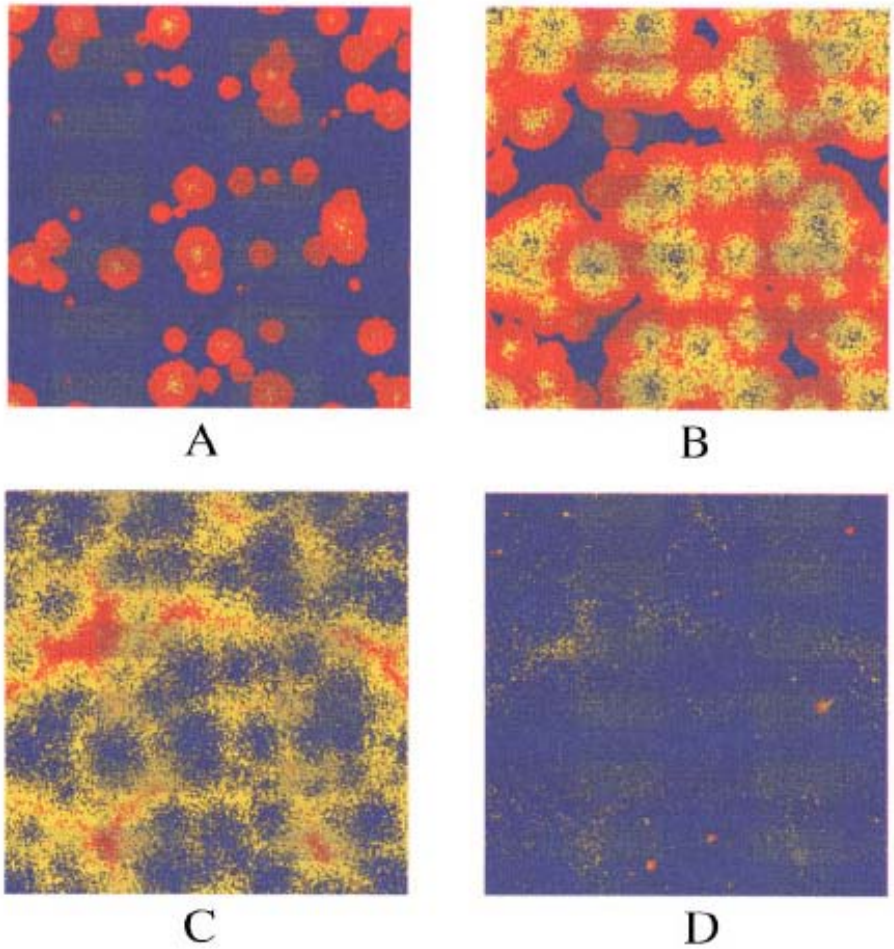

FIG. 5. (Color). Series of snapshots of a simulation grid of 1024×1024 unit cells, illustrating the observed synchronization mechanism. A number of reaction fronts arise due to CO desorption (A). When they have grown to full width, they collide (B), and extinguish one another (C). After this, an almost homogeneously transformed hexagonal phase results. On this surface, CO concentration builds up again, after which transformation into the 1×1 phase occurs (D). Red areas indicate oxygen on a 1×1 phase, blue areas indicate CO on a 1×1 phase. Yellow areas are empty hexagonal unit cells and green (mixed yellow and blue) areas show where CO is adsorbed on the hexagonal phase. Cellular structures very similar to picture (C) have been observed experimentally on Pt(110) surfaces (Ref. 19).

Gelten RJ, Jansen APJ, van Santen RA, et al., J. Chem. Phys. 108 (14) 5921-5934 1998

Kinetic Oscillations and Waves

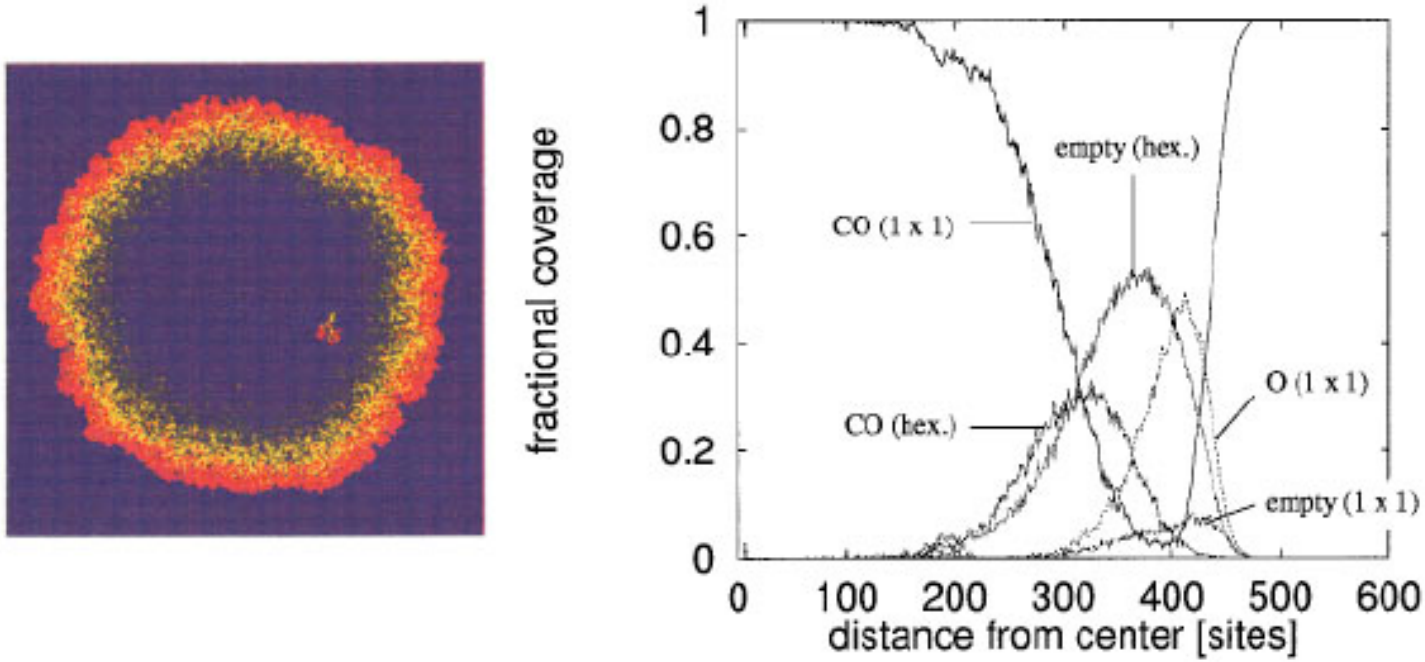

FIG. 8. (Color). Concentration profiles of adsorbate coverages and surface phases for a single reaction front. Note the initiation of a new reaction front inside the ring. This front is not initiated in the center of the primary front, but will be reshaped into a concentrical circle. Colors as in Fig. 5.

Gelten RJ, Jansen APJ, van Santen RA, et al., J. Chem. Phys. 108 (14) 5921-5934 1998

Kinetic Oscillations and Waves

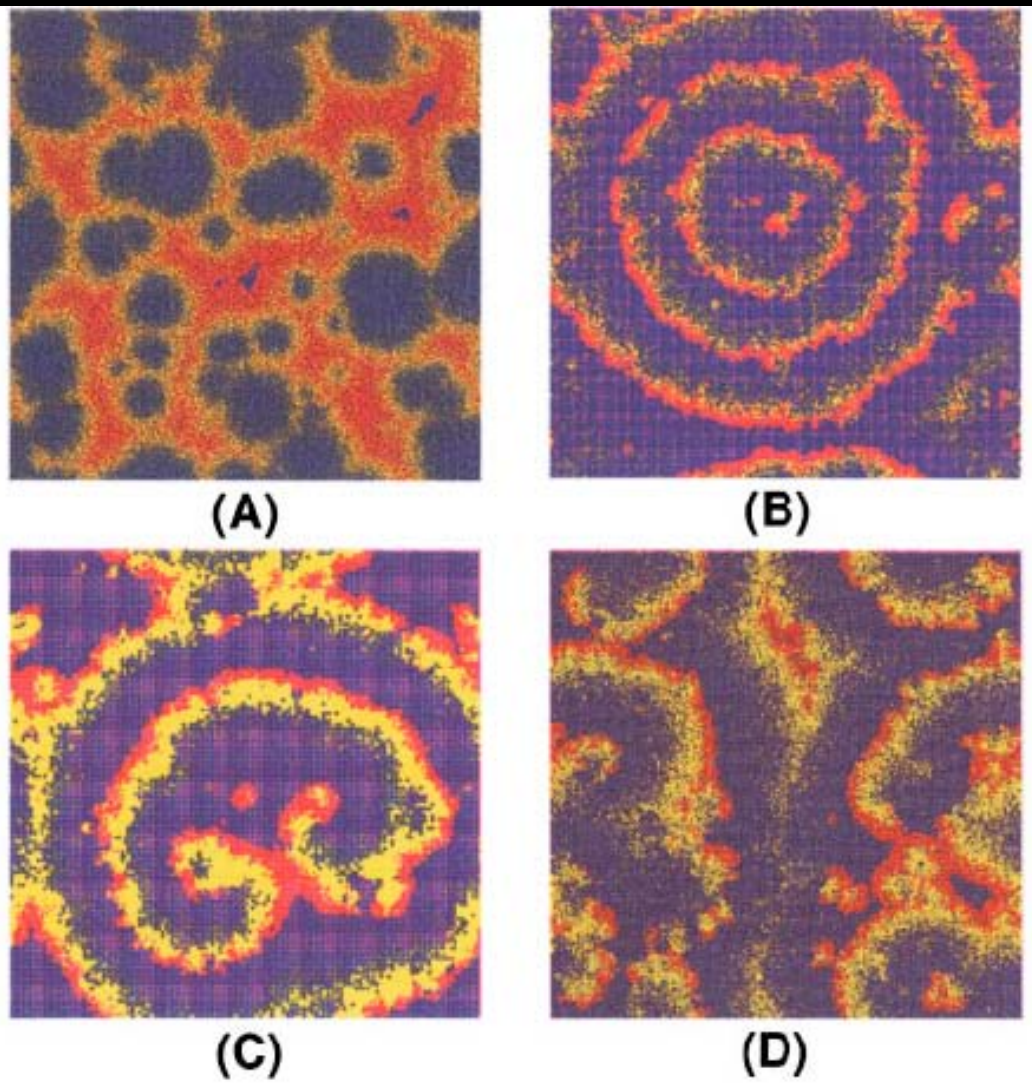

FIG. 7. (Color). Pattern formations during our simulations on grids of 1024 × 1024 unit cells. (A) Cellular patterns, (B) target patterns, (C) a double spiral, (D) turbulent patterns. The cellular patterns in this figure were obtained with diffusion. Colors as in Fig. 5.

Gelten RJ, Jansen APJ, van Santen RA, et al., J. Chem. Phys. 108 (14) 5921-5934 1998

More Detailed Reaction Kinetics

Apparent Activation Energies (kcal/mol)			*475 K*	*550 K*
1) O_2^*	$\longrightarrow$	$O_2 + *$	2-6	< 1
2) $O_2 + *$	$\longrightarrow$	O_2^*	<1	< 1
3) $O^* + O^*$	$\longrightarrow$	$O_2(g)$	-	83.7
4) $O_2(g) + 2^*$	$\longrightarrow$	$O^* + O^*$	29-33	23.7
5) CO^*	$\longrightarrow$	$CO(g) + *$	24-26	35.3
6) $CO(g) + *$	$\longrightarrow$	CO^*	1-2	0
7) CO_2^*	$\longrightarrow$	$CO_2(g) + *$	6-7	5.6
8) $CO_{2(}g) + *$	$\longrightarrow$	CO_2^*	-	0
9) CO_{2*}	$\longrightarrow$	$CO^* + O^*$	32	28.6
10) $CO^* + O^*$	$\longrightarrow$	CO_2^*	10-12	18.5
11) $CO_2 + O^*$	$\longrightarrow$	$CO^* + O_2^*$	-	0
12) $CO^* + O_2^*$	$\longrightarrow$	$CO_2(g) + O^*$	-	0
13) $O^* + O^*$	$\longrightarrow$	O_2^*	-	55.3
14) O_2^*	$\longrightarrow$	$2O^*$	2-6	

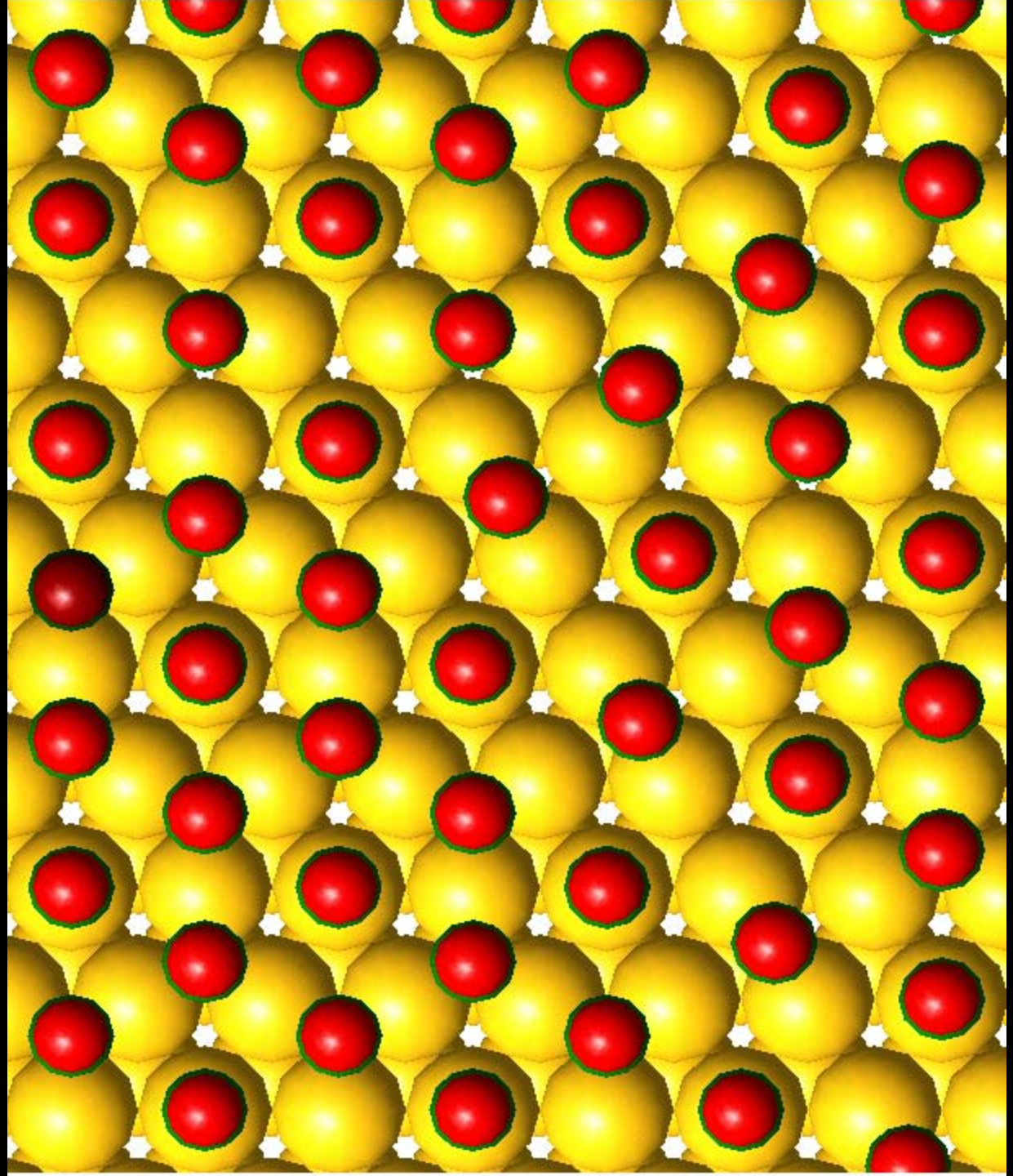

Surface Coverage T=475 K

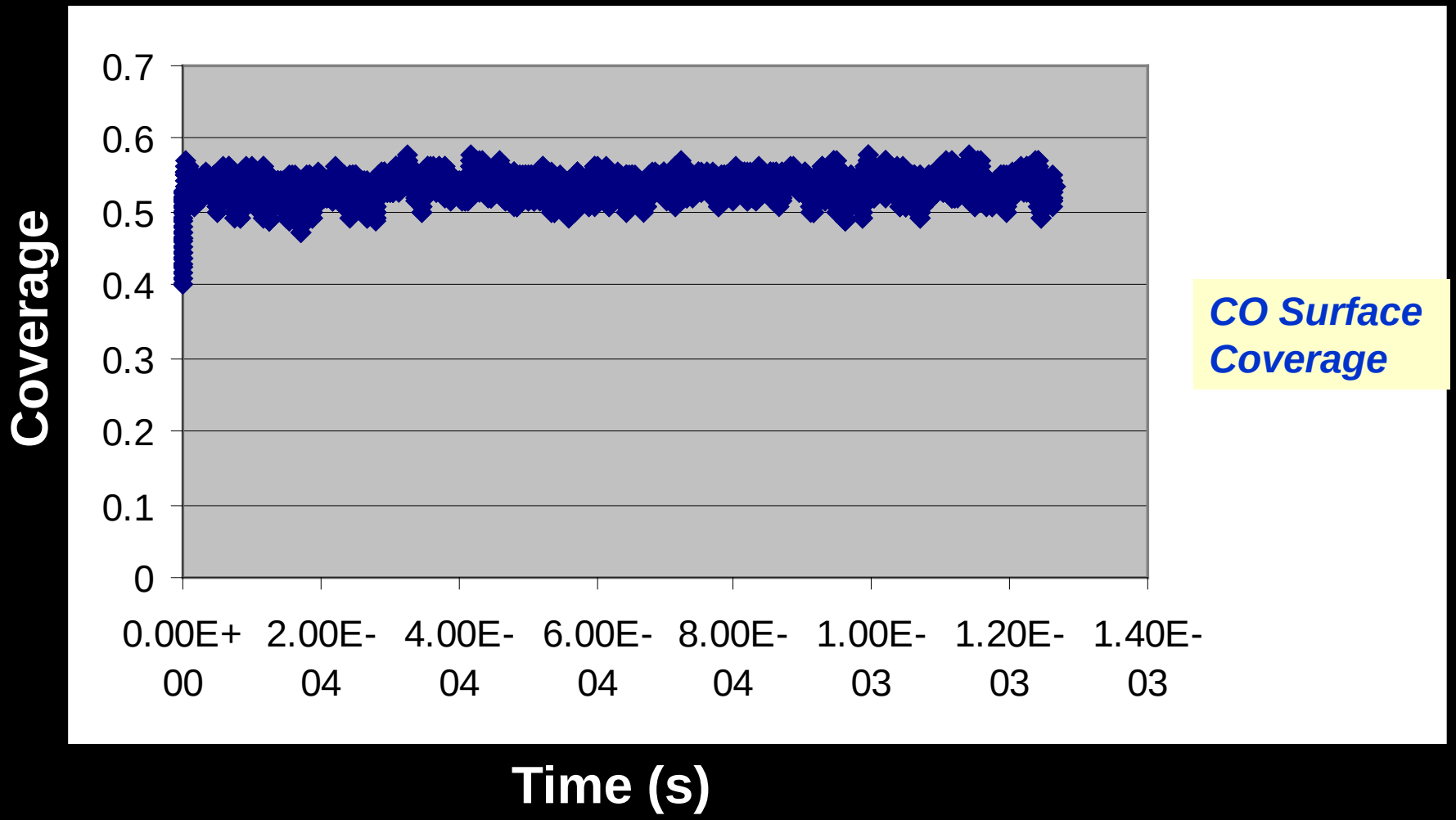

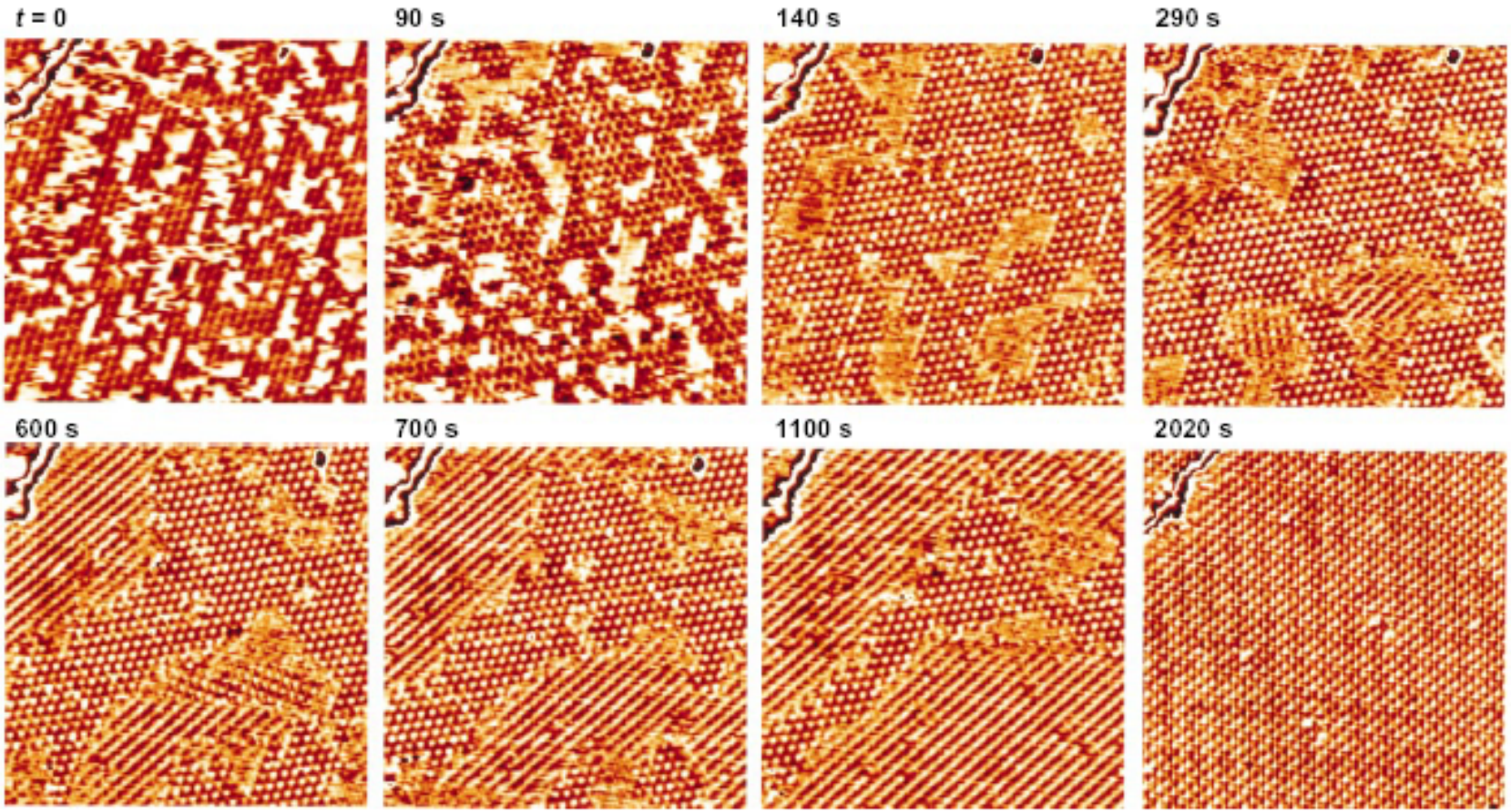

Fig. 1. Series of STM images, recorded during reaction of adsorbed oxygen atoms with co-adsorbed CO molecules at 247 K, all from the same area of a Pt(111) crystal. Before the experiment, a submonolayer of oxygen atoms was prepared (by an exposure of 3 Langmuirs O_2 at 96 K, a short annealing to 298 K, and cooling to 247 K), and CO was continuously supplied from the gas phase ($P_{CO} = 5 \times 10^{-8}$ mbar). At this pressure, the impingement rate of CO molecules is about 1 monolayer per 100 s, where the zero-coverage sticking coefficient on the empty and oxygen-covered surface is about 0.7 (*8*); the times refer to the start of the CO exposure. The structure at the upper left corner is an atomic step of the Pt surface. Image sizes, 180 Å by 170 Å; tunneling voltage (with respect to the sample), +0.5 V; tunneling current, 0.8 nA.

CO Oxidation over Pd (111)

Resulting Kinetics

Apparent Activation Energy

ΔE_A^{App} = 96.1 kJ/mol

Pre-exponential Factor

A = $3.8 \times 10^{13}\ s^{-1}$

Calculated barrier is consistent with results by Boudart over actual particles.

CO Oxidation on $Pt_{50}Ru_{50}$ Nanoparticle

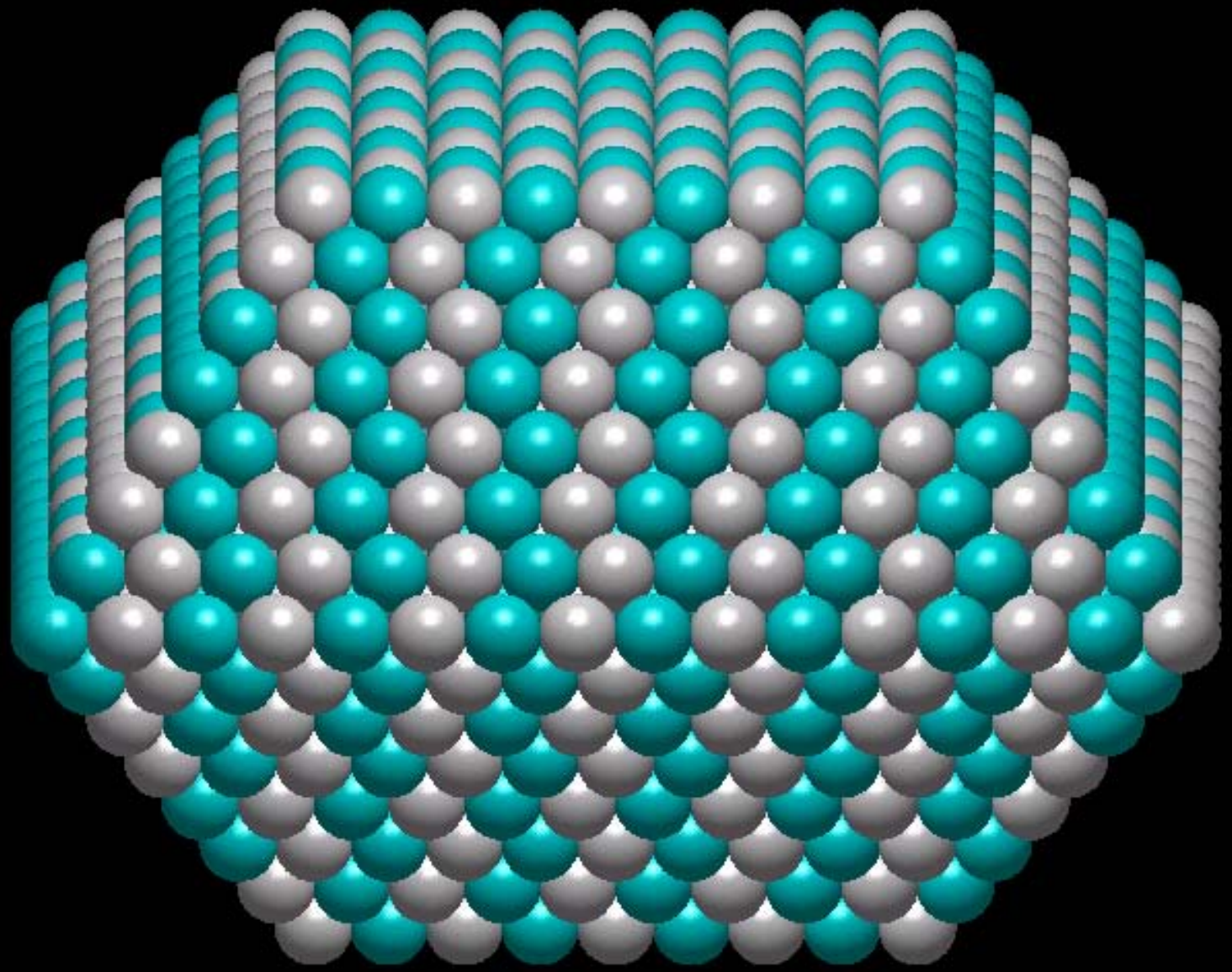

Simulating Electrocatalytic Systems

Butler-Volmer Kinetics

$$k_{oxidation} = k^0_{oxidation} \exp\left(\frac{\alpha e}{k_B T} E\right)$$

$$k_{reduction} = k^0_{reduction} \exp\left(\frac{-1(1-\alpha)}{k_B T} E\right)$$

E = potential

α = 0.5

Cyclic Voltametry

$$E(t) = E_0 + \nu t$$

ν = Sweep rate

$$k_{oxidation}(t') = k_{oxidation}(t) \exp\left(\frac{\alpha e\left[E(t') - E(t)\right]}{k_B T}\right)$$

$$k_{reduction}(t') = k_{reduction}(t) \exp\left(-\frac{\alpha e\left[E(t') - E(t)\right]}{k_B T}\right)$$

Determining the Current

$$i = e\left[\sum_{i=1}^{n-oxidation} v_i - \sum_{j1}^{n-reduction} v_j\right]$$

$$H_2O + *_{Ru} \rightleftharpoons OH_{Ru} + H^+ + e^-$$

$$H_2O + *_{Pt} \rightleftharpoons OH_{Pt} + H^+ + e^-$$

CO can react with a neighboring OH in four different w

$$CO_{Ru} + OH_{Ru} \rightarrow CO_2 + H^+ + 2*_{Ru} + e^-$$

$$CO_{Ru} + OH_{Pt} \rightarrow CO_2 + H^+ + *_{Ru} + e^-$$

$$CO_{Pt} + OH_{Pt} \rightarrow CO_2 + H^+ + 2*_{Pt} + e^-$$

$$CO_{Pt} + OH_{Ru} \rightarrow CO_2 + H^+ + *_{Pt} + *_{Ru} + e^-$$

Koper MTM, Lukkien JJ, Jansen APJ, et al., J. Phys. Chem. B 103 (26) 5522-5529, 1999

Influence of Ru Atomic Surface Configurations on CO Stripping

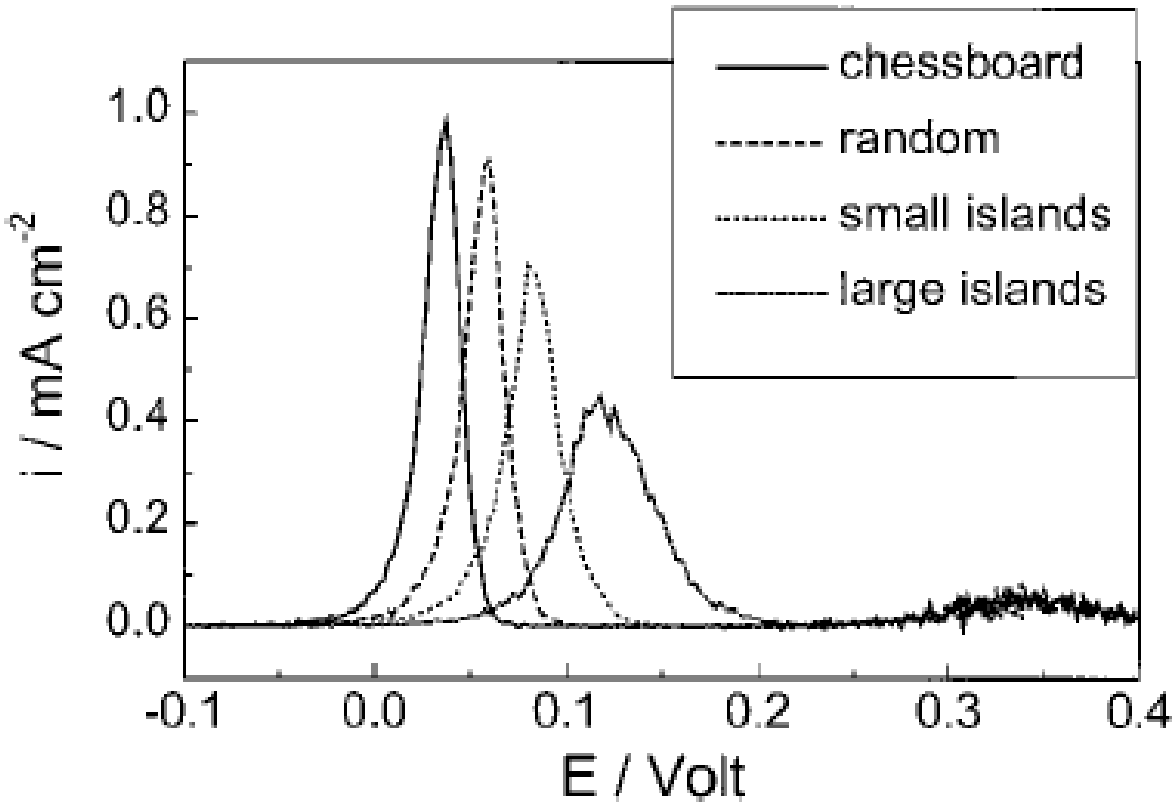

Figure 11. Comparison of the CO stripping voltammetry for the four different surfaces described in the text (and shown in Figure 10). Scan rate 50 mV/s. D = 1000.

Koper MTM, Lukkien JJ, Jansen APJ, et al., J. Phys. Chem. B 103 (26) 5522-5529, 1999

Influence of CO Diffusion on CO Stripping

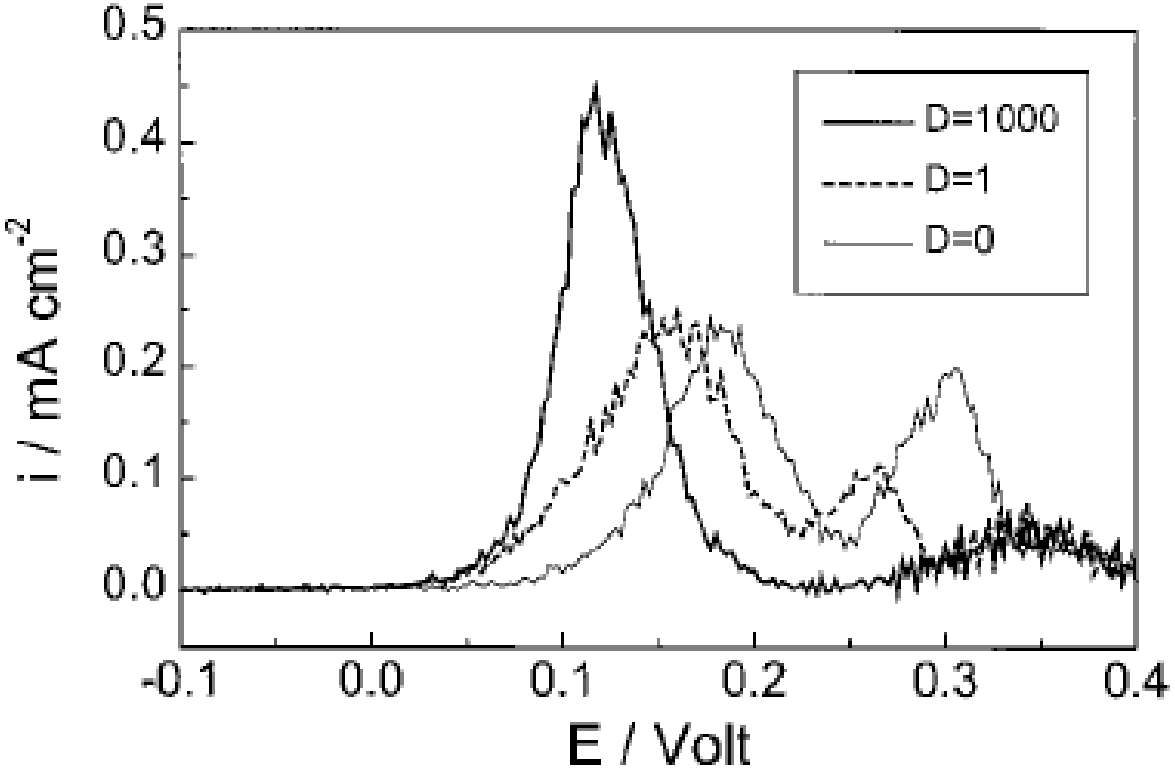

Figure 12. 2. Dependence of the CO stripping voltammetry for a x_{Ru} = 0.5 surface with large islands on the CO mobility *D*. Scan rate 50 mV/s.

Koper MTM, Lukkien JJ, Jansen APJ, et al., J. Phys. Chem. B 103 (26) 5522-5529, 1999

Theoretical Heterogeneous Catalysis

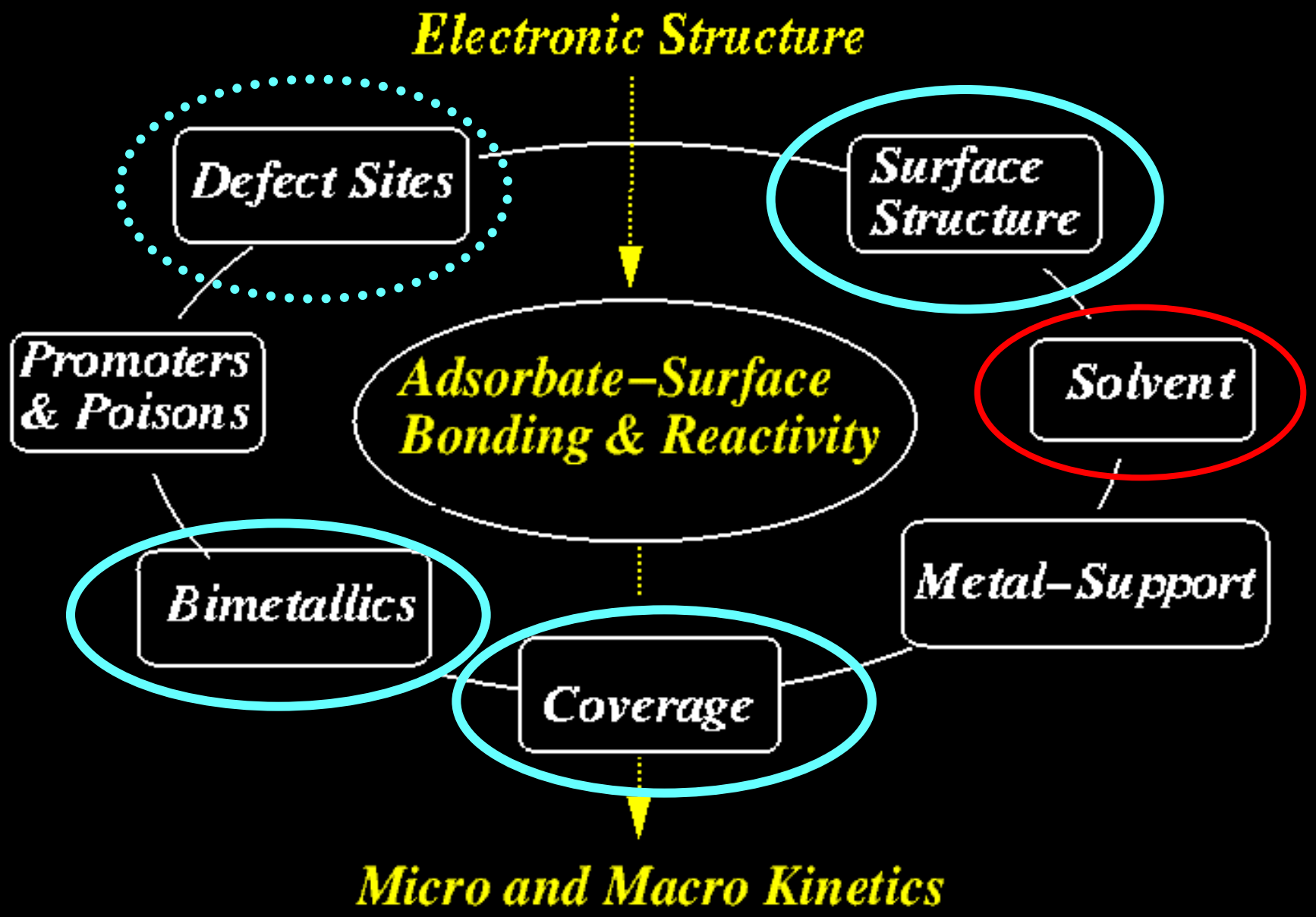

Acknowledgments

Dr. Qingfeng Ge
Dr. Donghai Mei
Dr. Priyam Sheth

National Science Foundation
DuPont Chemical Company
Dow Chemical Company
Accelerys
ARO MURI
Novodynamics

Professor Robert Davis (UVA)
Professor Rutger van Santen (TUE)
Professor Enrique Iglesia (UCB)
Dr. Laurent Kieken
Dr. Jan Lerou

Kinetic Monte Carlo Simulation

Ignores the local electronic interactions that occur and simulates the elementary kinetic processes.

Adsorption, Diffusion, Deposition, Reaction, Desorption

Follows the time-dependent changes in surface structure.

$$\Delta t_v = -\frac{\ln(RN)}{\sum_{i=1}^{Nevents} k_i}$$

Δt_v is the time for the next kinetic event to occur

k_i is the rate constant associated with event i.

The reaction event that follows is chosen by sampling from the cumulative probability distribution of all conceivable events.

$$S = k_i \Big/ \sum_{i=1}^{Nevents} k_i$$

Influence of the Reaction Environment

Much to learn be learned from and taught about biological systems.

Intelligent Nanoscale Materials

Algorithm Specifics

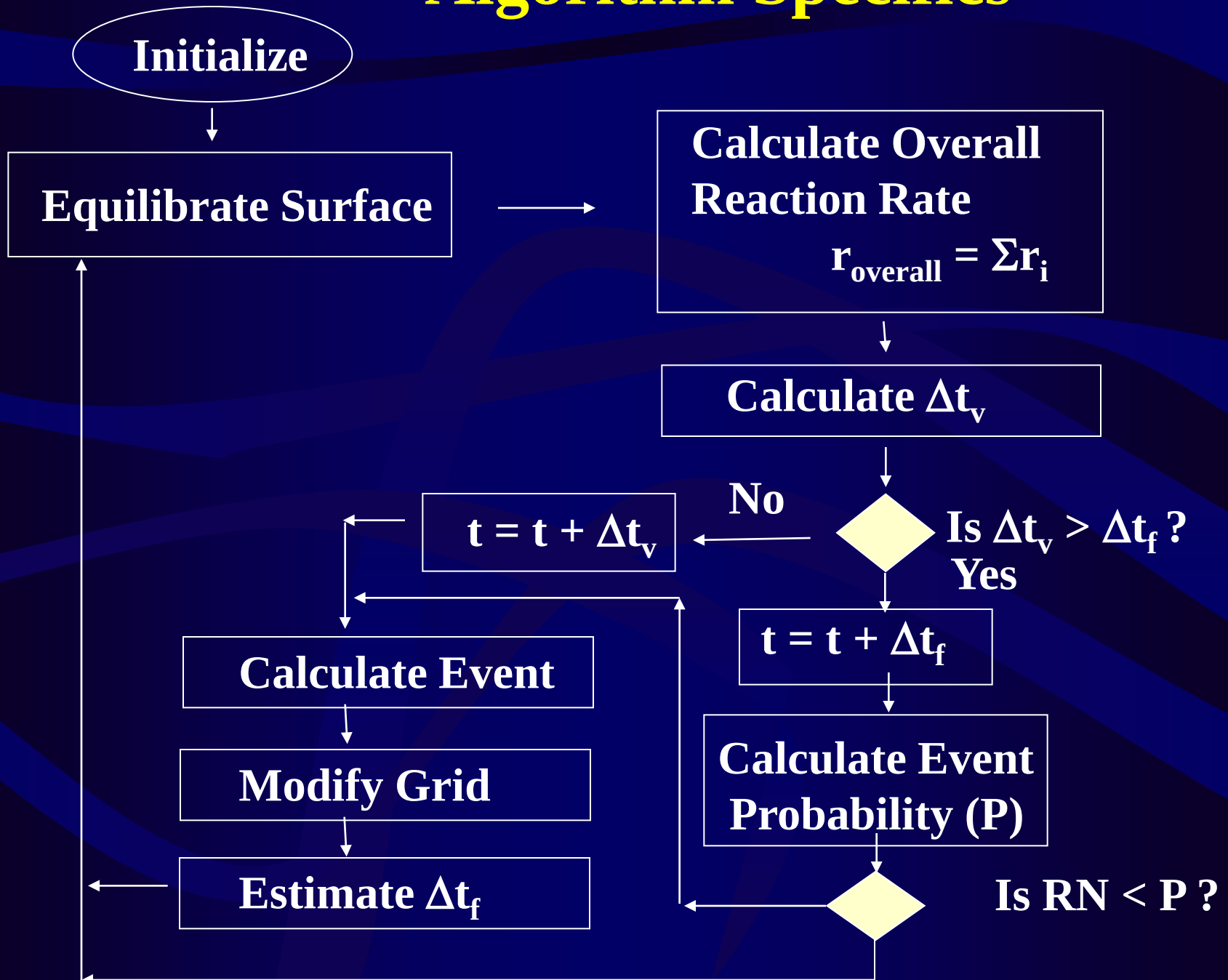

Extended Bond Order Conservation

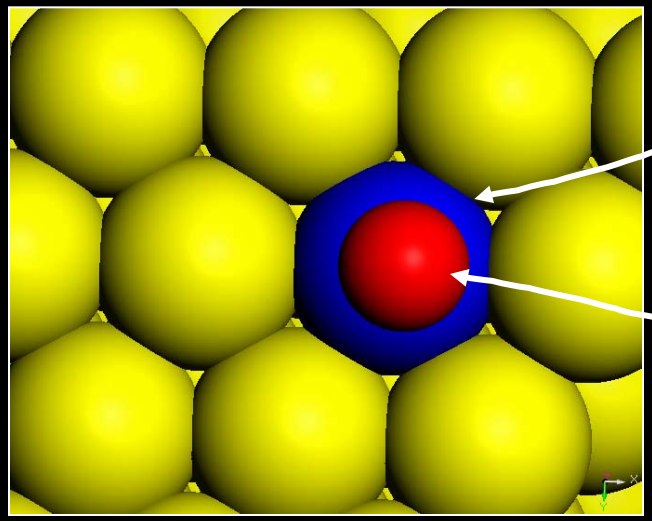

Metal atom of interest
(co-ordination # = 9)

Adsorbate atom

$$Et = E(BOC) + E(MBOC)$$

$$E(BOC) = a_2|x^2 - 2x|$$

$$E(MBOC) = b_2|y^2 - b_3.y|$$

$$Q_A(n) = Q_A(2-1/n) + n.b_2.G.\ [\ (G/\text{coordn}\ \#) - b_3\ ]$$

Heterogeneous Catalysts

Metastable nanoscale architectures.

Involve self-assembly of reactants at the active site

Controlled by the active site and its environment.

Readily regenerated.

Living System